

# Okhotsk Sea and Polar Oceans Research

**Volume 8 (2024)**



**Okhotsk Sea and Polar Oceans Research Association**

**Mombetsu City, Hokkaido, Japan**

**Vol. 8**

# General Information for OSPOR

for OSPOR Vol. 8 (2024)  
(July 2023)

## 1. Aims and Scope

Okhotsk Sea and Polar Oceans Research (OSPOR) is published by the Okhotsk Sea and Polar Oceans Research Association (OSPORA).

Since 1986 the Okhotsk Sea and Cold Ocean Research Association (OSCORA) has held the International Symposium at Mombetsu, Hokkaido, in Japan every February and has released its proceedings over 35 years. In 2017 OSCORA changed to OSPORA, because the Symposium scope was broadened to include the polar oceans (the Arctic and Antarctic Oceans), the Arctic passages, global warming, and environmental change in Polar Regions.

OSPORA started a reviewed papers system from the 2017 Symposium. The papers are refereed by multiple reviewers, published in the proceedings of the Symposium with a title of 'Article' or 'Review', and opened on the OSPOR website.

## 2. Subjects covered by OSPOR

- 1) Environment of Okhotsk Sea
- 2) Meteorology and oceanography in polar regions
- 3) Cold region engineering
- 4) Arctic sea routes
- 5) Global warming and environment change
- 6) Remote sensing
- 7) Snow, ice and human life
- 8) Other topics about Okhotsk Sea and Polar Oceans

## 3. Editorial Policy of OSPOR

We intend to publish two types of papers;

- 1) **Article**, containing original scientific materials and results, not submitted for publication elsewhere,
- 2) **Review**, containing an overview of previous activities, projects and workshops with an outlook of a specific category.

Each of them will be peer-reviewed.

## 4. Editorial Board

Period: August 2022 - August 2024

Editor-in-Chief : Hiromitsu Kitagawa (Ocean Policy Research Institute, Japan)

Editors : Hajo Eicken (University of Alaska Fairbanks, USA)

Hiroyuki Enomoto (National Institute of Polar Research, Japan)

Natsuhiko Otsuka (Hokkaido University, Japan)

Yutaka Michida (University of Tokyo, Japan)

Humio Mitsudera (Hokkaido University, Japan)

Koji Shimada (Tokyo University of Marine Science and Technology, Japan)

Shuhei Takahashi (Okhotsk Sea Ice Museum of Hokkaido, Japan)

Hajime Yamaguchi (National Institute of Polar Research, Japan)

## 5. OSPOR website

Temporal website: <http://okhotsk-mombetsu.jp/okhsympo/top-index.html>

E-mail: [momsys\(at\)okhotsk-mombetsu.jp](mailto:momsys@okhotsk-mombetsu.jp)

# Okhotsk Sea and Polar Oceans Research Volume 8 (2024)

## Contents

### [Articles]

Intra-seasonal and interannual variation of snowfall and rainfall during winter in Rikubetsu, inland Hokkaido, Japan ···· 1 – 7

Naohiko HIRASAWA and Hiroyuki KONISHI  
(<https://doi.org/10.57287/ospor.8.1>)

Intra-seasonal and interannual variations of sea ice along the Okhotsk coast of Hokkaido from the viewpoint of atmospheric circulation ···· 8 – 16

Yuki ASAZUMA, Masaya KURAMOCHI, and Hiroaki UEDA  
(<https://doi.org/10.57287/ospor.8.8>)

Laboratory experiments on spray icing with urea-doped water using flat and cylindrical specimens ···· 17 – 23

Toshihiro OZEKI, Takatoshi MATSUZAWA, Shingo NOMURA,  
Satoru ADACHI, Taiki TOKUDOME and Akihisa KONNO  
(<https://doi.org/10.57287/ospor.8.17>)

### [Review]

Frederick William Beechey's Narrative of the Voyage of the Blossom to the Pacific and the Arctic ···· 24 – 28

Gaston R. DEMARÉE and Yoshio TAGAMI  
(<https://doi.org/10.57287/ospor.8.24>)



# Intra-seasonal and interannual variations in snowfall and rainfall during winter in Rikubetsu, inland Hokkaido, Japan

Naohiko HIRASAWA<sup>1,2</sup> and Hiroyuki KONISHI<sup>3</sup>

<sup>1</sup> National Institute of Polar Research, Tachikawa, Tokyo, Japan

<sup>2</sup> Department of Polar Science, School of Multidisciplinary Sciences, SOKENDAI (The Graduate University for Advanced Studies), Tachikawa, Tokyo, Japan

<sup>3</sup> Division of Math, Sciences, and Information Technology in Education, Osaka Kyoiku University, Osaka, Japan

(Received October 1, 2023; Revised manuscript accepted December 31, 2023)

## Abstract

Global warming is likely to increase precipitation and the relative proportion of rainfall to precipitation. Since relatively few continuous and independent observations of snowfall and rainfall have been conducted worldwide, it is difficult to clarify the likelihood of future changes in the proportion of snow versus rainfall. Low-cost disdrometers, which have become more ubiquitous in recent years, can record snowfall and rainfall separately based on the characteristics of the precipitation particles. In this study, snowfall and rainfall amounts were investigated using disdrometer measurements for the winters from 2013 to 2023 in Rikubetsu (43.5°N, 143.8°E), Hokkaido, Japan. It represents the current status on snowfall in one of the southernmost regions of the Arctic. The results show that the total winter precipitation in each year ranged from 101.9 to 399.6 mm. Rainfall ranged from 5.9 to 80.2 mm, and therefore accounted for 17% of the total precipitation, 96% of which occurred in December and March. Rainfall accounted for 2% in January and February, and 27% in December and March, respectively. Large snowfall and rainfall events contributed significantly to total winter precipitation, and these events were associated with rising temperatures associated with synoptic-scale disturbances. Snowfall occurred when temperatures were below freezing after warming, and rainfall occurred when temperatures were above freezing. It is considered that future changes in temperatures during synoptic-scale disturbances will play a key role in the amount of rainfall in Rikubetsu as the climate changes.

**Key words:** snowfall, liquid precipitation, solid precipitation, climatological monitoring, disdrometer, Rikubetsu

## 1. Introduction

It has been hypothesized that global warming will promote an increase in water vapor, leading to an increase in precipitation. For example, in an analysis based on the Clausius-Clapeyron equation, Trenberth *et al.* (2003) proposed that the rate of increase in atmospheric water vapor capacity is approximately 7% K<sup>-1</sup>, which implies that the overall rate of the increase in precipitation should follow the same trend (Clausius-Clapeyron scaling). This idea has subsequently been corroborated by several studies that were conducted primarily on rainfall (*e.g.*, Nayak and Takemi, 2020). Although the rate of the increase in snowfall remains an issue in the future, even in the Arctic region (north of 70°N) where snowfall is the main component of precipitation, precipitation has increased throughout the 20th century and is expected to increase at an escalating rate in the 21st century (*e.g.*, Vihma *et al.*, 2016).

Another concern related to the impact of global warming on precipitation is that it will reduce the frequency of snowfall, *i.e.*, the frequency of rainfall will

increase. According to McCrystall *et al.* (2021), the fraction of snowfall in the Arctic decreased during the 20th century, and climate models (CMIP 5 and 6) predict that the relative contribution of snowfall to total precipitation will continue to decrease during the 21st century. The findings of their study showed that rainfall is expected to account for more than 50% of the total precipitation in autumn (September–November) by 2050. The timing of when rainfall is expected to exceed snowfall varies by season and region, but a common feature of current estimates is that there will be an increase in the proportion of future rainfall.

In Japan, there are few long-term data on snowfall rate as water equivalent, but analyses have been attempted using data from the Japan Meteorological Agency (JMA) and other sources. The JMA records total amount of rainfall and snowfall, and snow depth, with snow depth and depth of new snowfall mainly being used as surrogate data for snowfall (*e.g.*, Takahashi, 2021; Kawase *et al.*, 2023). Takahashi (2021) used data from weather stations throughout Japan to clarify in

detail the trend in the change of snowfall from 1961 to 2012. Most of the weather stations in Honshu, Shikoku, and Kyushu have recorded a decreasing trend in snowfall, while in Hokkaido, some stations show an increasing trend and others show a decreasing trend. Kawase *et al.* (2023) investigated historical snowfall changes in Japan from 1959 to 2020 with a dynamical downscaling analysis forced by the Japanese 55-year Reanalysis data (JRA-55). The trends observed in the maximum snow depth and the maximum snowfall (increment in daily snow depth) in Hokkaido were generally insignificant, which differed slightly from the results reported by Takahashi (2021). The reason for the disparity between the findings of the studies could be attributed to differences between modeled values and observations. Kawase *et al.* (2021) used a climate model to calculate changes in snowfall in Japan due to global warming (RCP 8.5 and 2.6). In both cases, the change in precipitation is not pronounced in Hokkaido, but shows a trend from snowfall to rainfall before December and after February.

As global warming progresses, an increase in precipitation and the relative proportion of rainfall is expected to increase in Hokkaido and other snowfall regions. These changes will affect people's way of life in the future and are also important as one of the indicators of the state of the global climate. However, historically, few independent rainfall and snowfall observations have been conducted, and we do not have accurate and sufficient information about rainfall and snowfall events.

Disdrometers measure the size and fall velocity of precipitation particles, and based on the characteristics of these two parameters, rainfall and snowfall can be separated and their respective amounts can be estimated. Recent technological innovations have led to the commercial availability of low-cost disdrometers, and observations using these instruments are increasing worldwide. Based on these observations, it is meaningful to obtain information on rainfall and snowfall separately in snowfall areas in order to evaluate the potential for changes in the characteristics of these events in future.

In this study, we investigated the intra-seasonal and inter-annual variations in snowfall and rainfall amounts in Rikubetsu, Hokkaido, Japan, using a disdrometer. The observations were conducted from the winter of 2013 (December 2012 to March 2013) to 2023. Section 2 presents the observation site and the details of the measurements in Rikubetsu, Section 3 examines intra-seasonal and inter-annual variations in data, Section 4 presents case analyses, and Section 5 provides a summary of our findings.

## 2. Observation site and measurements

We have been conducting snowfall and meteorological measurements at an observation site in Rikubetsu (43.5°N, 143.8°E, 217 m above sea level)

since 2012 (Figs. 1a and c). Rikubetsu is located on the eastern side of the central mountain range (white broken line in Fig. 1a) in Hokkaido. The mountains separate the site from the Sea of Japan side of the island, which typically experiences heavy snowfall during the Asian winter monsoon. During the heavy snowfall on the Sea of Japan side of Hokkaido, most of the areas on the Pacific Ocean side, including Rikubetsu, generally experience clear skies. Snowfalls in Rikubetsu are mainly attributed to frontal activity associated with synoptic-scale disturbances passing through the region (*e.g.*, Kawase *et al.*, 2023). Rikubetsu is a slightly elevated area that extends from Kitami city in the north to Obihiro city in the south and is one of the coldest areas in Japan (Sorai *et al.*, 2016), with daily winter minimum air temperatures often reaching approximately  $-30^{\circ}\text{C}$ . This cold region is valuable as a test site for Arctic and Antarctic snowfall observations. Therefore, we have continued snowfall observations in Rikubetsu since 2012.

The observations were part of the WMO-directed Solid Precipitation Inter-Comparison Experiment (SPICE) that ran from 2013 to 2015 (Nitu *et al.*, 2018). The main objectives of SPICE were to understand the accuracy of the snowfall rate and snow depth observations being conducted in each country, to propose correction methods, and to learn about the performance of new instruments. The data used in this study were collected using a disdrometer named Laser Precipitation Monitor (LPM) manufactured by Theis, Germany (Fig. 1b). The LPM data were analyzed for the SPICE project (Hirasawa *et al.*, 2018) and also used to analyze diurnal variations in precipitation by Hirasawa and Konishi (2023). Over the two-year SPICE period, the observed values of this LPM were slightly overestimated as ratios of 1.1 and 1.2 to the SPICE reference data (DFIR: Double Fence Intercomparison Reference).

The LPM was placed in the center of a wooden double fence for wind protection (Fig. 1c). The double fence was constructed according to the standard specifications for measuring inter-comparison data in SPICE. This placement of the LPM was employed to increase the accuracy of precipitation measurements by suppressing the contributions of blowing snow due to strong winds during synoptic-scale disturbances. The LPM measures the size and fall velocity of precipitation particles, and based on correlations of their distribution, discriminates between rainfall (liquid precipitation) and snowfall (solid precipitation) (Gunn and Kinze, 1949), and then determines the relative amounts of each. Gunn and Kinze (1949) is an older results, however, it is still one of the most reliable empirical formulas today. In addition, the algorithm discriminates precipitation as snowfall when the ambient temperature is below  $-4^{\circ}\text{C}$  and rainfall when the temperature is above  $9^{\circ}\text{C}$ . Since drizzle consisting of supercooled water droplets can

cause rain even below freezing, we also believe it is possible to place the snowfall decision at  $-4^{\circ}\text{C}$ . The accuracy of the rain/snow discrimination algorithm was recently verified by Pickering *et al.* (2019).

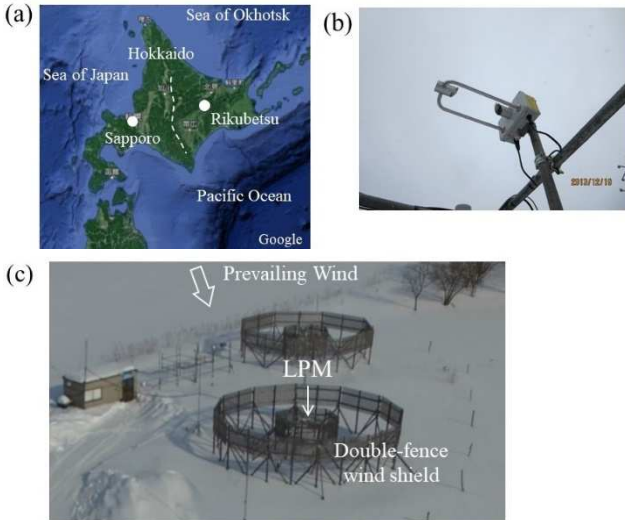


Fig. 1 (a) Map of Hokkaido showing the location of Rikubetsu and the topography of the region. The white dashed line indicates the mountain range that divides the island into the Sea of Japan side and the Pacific Ocean side. (b) Disdrometer, LPM. (c) Landscape surrounding observation site.

Solid and liquid precipitation can occur simultaneously or separately within the same precipitation events. In this study, such measurements will be referred to as snowfall and rainfall, respectively. In the figures, however, the terms "solid" and "liquid" are used.

An automatic observation system operated by JMA is located approximately 2 km away from our observation site, where temperature, humidity, wind direction and speed, precipitation amount (total of rainfall and snowfall), and snow depth are measured. This study refers to these data.

In this study, winter was defined as the period extending from December 1 to March 31. Observations spanned the period from the 2013 winter season beginning in 2012 until the 2023 winter beginning in 2022. However, data for the 2022 winter season were excluded from the analysis due to a malfunction of the equipment. Hourly and daily data were used for the analyses in this study. For the ten winters included in the analysis, periods during which no data were obtained for more than 12 hours occurred from 9:00 on December 5 to 14:00 on December 21 for the 2013 winter season and from 0:00 on February 14 to 8:00 on February 18 for the 2021 winter season. Times are in Japan Standard Time (JST).

### 3. Amount of snowfall and rainfall in each winter

#### 3.1 Inter-annual variation over the entire winter season

Figure 2a shows a time series of cumulative precipitation for the winter season from 2013 to 2023. The highest precipitation recorded was 399.6 mm in the 2015 winter and the lowest was 101.9 mm in the 2021 winter. Although the JMA data underestimated the LPM measurements, the two datasets were generally consistent with respect to their inter-annual variability. Average precipitation was 204.7 mm as recorded by the LPM and 134.9 mm by the JMA, respectively, giving a ratio of 65.9%. Hirasawa *et al.* (2018) showed that the underestimation of the JMA instrument is due to reduced capture of precipitation particles by wind and further evaporation.

Snowfall (solid precipitation) was greater than rainfall (liquid precipitation) throughout the winter in all years. The mean value obtained for snowfall was 168.9 mm, with a maximum of 355.5 mm in the 2015 winter and a minimum of 90.5 mm in the 2021 winter. The mean value obtained for rainfall was 35.7 mm, with a maximum of 80.2 mm in the 2018 winter and a minimum of 5.9 mm in the 2017 winter. The relative proportion of rainfall (Fig. 2b) varied from 4.1% in the 2017 winter to 36.4% in the 2018 winter, and the mean was 17.0%.

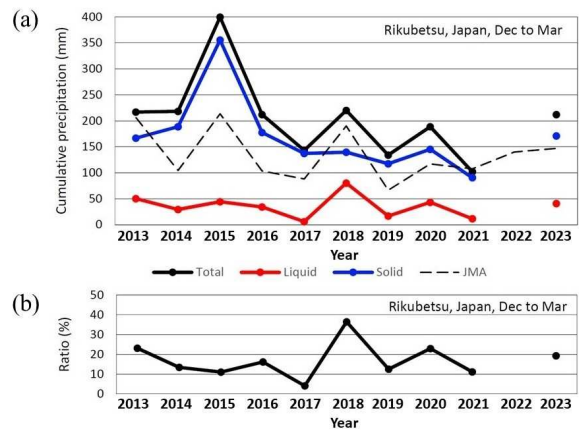


Fig. 2 (a) Time series of cumulative precipitation for the winter season from 2013 to 2023. The black, red, blue, and black dashed lines indicate total precipitation, liquid precipitation, and solid precipitation measured by the LPM, and total precipitation by the JMA, respectively. (b) Time series of liquid precipitation as a percentage of total precipitation.

#### 3.2 Intra-seasonal variation

Figure 3 shows time series of daily precipitation, with all years overlaid. Snowfall was more frequent than rainfall, often with smaller daily precipitation amounts, and was generally distributed evenly from December to March. Rain rarely fell in January and February during the observation period. This is characteristic of the

climate in Rikubetsu, which is one of the coldest regions in Japan.

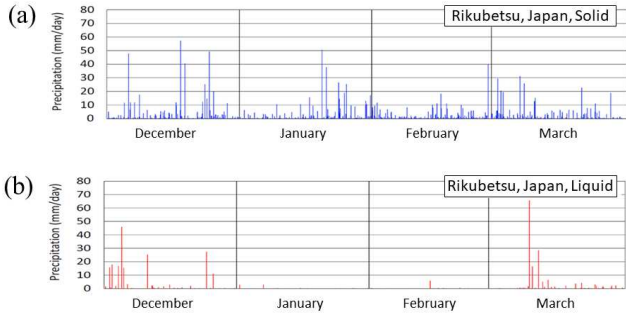


Fig. 3 Time series of daily precipitation overlaid for all years for (a) solid precipitation and (b) liquid precipitation.

Figures 4 and 5 show time series of cumulative precipitation amounts in December and March, and January and February from the 2013 winter to the 2023 winter. The cumulative rainfall in December and March in each year (red line in Fig. 4a) was almost the same as that of all years, while the cumulative total precipitation for the two months (black line in Fig. 4a) was less than that in all years. Thus, the relative proportion of rainfall during this period was greater than that of all years (Fig. 4b). The mean value was 26.6%, with a maximum of 48.4% in the 2018 winter and a minimum of 5.8% in the 2017 winter.

On the other hand, cumulative rainfall in January and February (red line in Fig. 5a) was very low compared to that in December and March, with a mean value of 1.6 mm, a minimum of 0.0 mm in the 2013 winter, and a maximum of 6.2 mm in the 2016 winter. The relative proportion of rainfall was also very low compared to December and March, with a mean value of 1.6%, a minimum of 0.0% the 2013 winter, and a maximum of 5.1% in the 2020 winter.

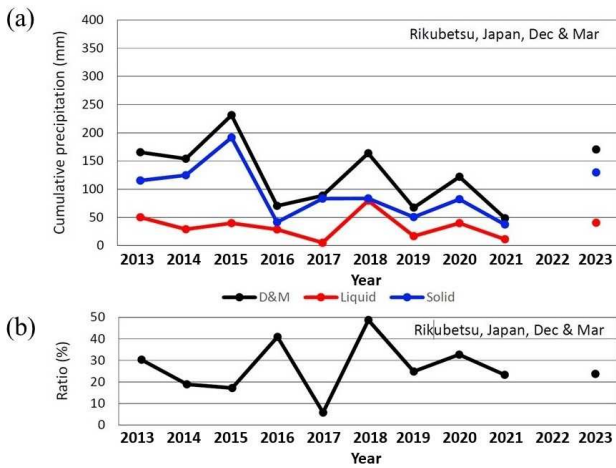


Fig. 4 Same as Fig. 2, but for December and March.

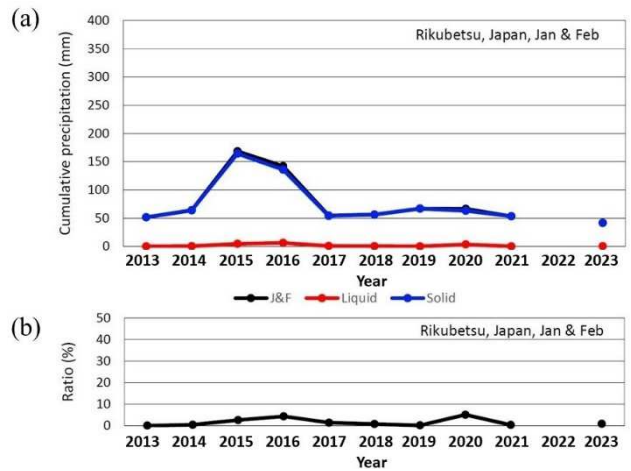


Fig. 5 Same as Fig. 2, but for January and February.

These findings indicate that in the current climate, almost all of the winter rainfall in Rikubetsu occurs in December and March, and that rainfall during those months accounts for 95.6% of the total winter rainfall.

Years with high snowfall and years with high rainfall were different, with each contributing to the variation in winter precipitation. For example, during the 2015 winter, multiple relatively large snowfall events that occurred from December to February (Fig. 6a) increased precipitation throughout the winter (Fig. 5a) and contributed to the annual maximum observed in this study (Fig. 2a). The 2016 winter had a notable snowfall event in January (Fig. 6b), which was the second highest precipitation event in January and February (Fig. 5a) observed over the analysis period, but no other notable precipitation events were observed. In the 2018 winter, a rainfall event measuring 65.6 mm was observed on March 9 (Fig. 6d). This event elevated the overall winter rainfall to the highest level within the analysis period (Fig. 5a), but snowfall was negligible. However, during the winter months, one, or possibly a few, relatively significant precipitation events, whether annual snowfall or annual rainfall, considerably influenced the overall amount of precipitation.

In the 2017 winter (Fig. 6c), there were no significant rainfall events in December and March. The 2017 winter season had a significantly lower percentage of rainfall. This could be partially attributed to lower temperatures in December (-8.4°C compared to the 10-year average of -7.5°C) and March (-2.5°C, -1.6°C). The small precipitation amounts for individual precipitation events may reflect the low activity of the synoptic-scale disturbances, which are accompanied by warm air advection, and therefore less rainfall. Such inter-annual variability occurs in association with hemispheric-scale atmospheric circulation. Further investigation of this is a future work.

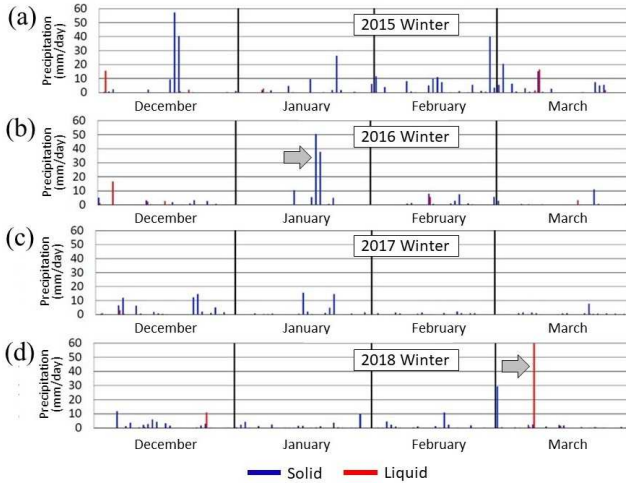


Fig. 6 Time series of daily rainfall and snowfall for selected years. Blue bars indicate daily snowfall and red bars indicate daily rainfall. (a) The 2015 winter, (b) the 2016 winter, and (c) the 2017–18 winter. Horizontal arrows in (b) and (c) indicate significant precipitation events, which are discussed in detail in Section 4.

4. Case studies

Here, we examine the surface meteorological and synoptic-scale atmospheric fields for significant snowfall and rainfall events on January 19–20, 2016 (Fig. 6b) and March 9, 2018 (Fig. 6c), respectively.

Figure 7 shows the surface weather maps for both cases. In each case, a synoptic-scale disturbance passed close to Hokkaido and caused precipitation.

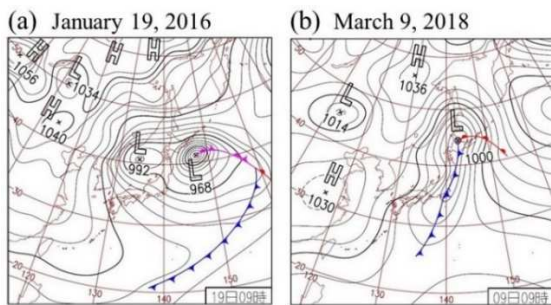


Fig. 7 Surface weather map, derived from the JMA, for (a) a snowfall event on January 19, 2016 and (b) a rainfall event on March 9, 2018.

Figures 8 and 9 show time series of precipitation and surface meteorological parameters. On January 19–20 and March 9, when precipitation occurred (Figs. 8a and 9a), the diurnal variation in temperature was moderated and temperatures remained relatively high (red lines in Figs. 8b and 9b). These conditions were likely attributed to warm air advection associated with the disturbances and the suppression of radiative cooling due to cloudy skies. Temperatures were the main factor separating the snowfall observed on January 19–20 from the rainfall

observed on March 9. In the former case, temperatures were relatively high, but still below the freezing point, while in the latter case, they were above the freezing point. Closer examination of the precipitation observed on March 9 reveals that snowfall was initially observed, and the temperature at that time was below the freezing point. The LPM data appear to have distinguished between the snowfall and rainfall with considerable accuracy based on the characteristics of the measured precipitation particles.

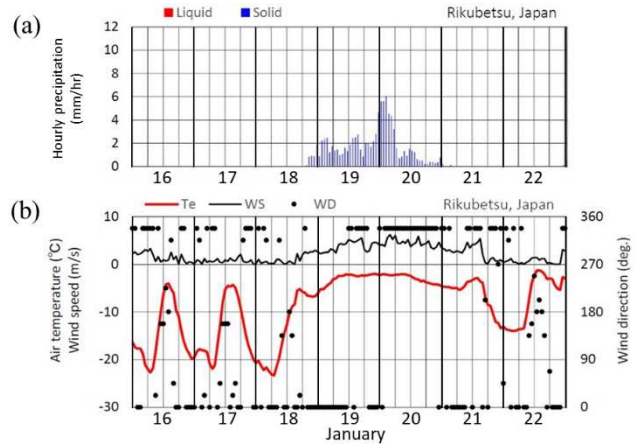


Fig. 8 Time series of (a) hourly rainfall (red bars) and snowfall (blue bars), and (b) surface air temperature (red line, °C), wind speed (black line, m/s), and wind direction (black circles, deg.) are shown for the period January 16 to 22, 2016.

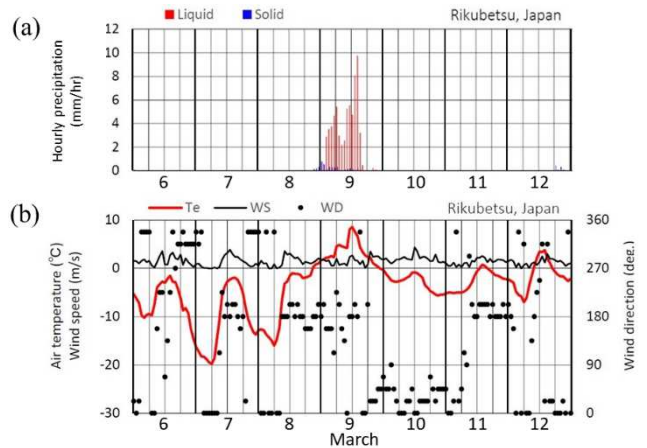


Fig. 9 Same as Fig. 8, but for March 6 to 12, 2018.

Finally, we examined the causes of this temperature difference, which is an important factor in distinguishing between the snowfall and rainfall. First, it is considered that temperature differences associated with seasonal progression (*i.e.*, intra-seasonal variation) would be involved. Focusing on the diurnal variation in temperature before each precipitation event, the minimum and maximum temperatures were below -

20°C and below -5°C before the snowfall event, but above -20°C and above -5°C before the rainfall event, respectively. The average daily temperature was -14.0°C on January 17 and -10.6°C on March 7, a difference of 3.4°C. Temperatures during the snowfall event were above -3.4°C from 6:00 JST on March 19 to 15:00 JST on March 20, and remained above -2.5°C for a relatively long time during that period. If the same phenomenon had occurred during a period of higher ambient temperatures, then it is considered likely that rainfall would have occurred.

In addition, the location of the synoptic-scale disturbance is also considered to be important. In the case of snowfall, the main disturbance passed over the Pacific Ocean to the east of Hokkaido, and in the case of rainfall, it passed over Hokkaido and was closer to Rikubetsu. The rainfall occurred when southerly winds blew, presumably during the passage of a cold front associated with the disturbance. In other words, rainfall occurred during pronounced warm air advection on a synoptic-scale, even though the associated wind speeds were not remarkably high. In contrast, in the case of the snowfall, northerly winds continued to blow throughout the event. Since Rikubetsu was to the north of the disturbance, it was not strongly affected by the warm air advection conditions.

## 5. Conclusion

This study investigated intra-seasonal and inter-annual variations in snowfall and rainfall amounts in Rikubetsu using disdrometer (LPM) data that were collected over the winters of 2013 (December 2012 to March 2013) to 2023. The LPM distinguishes between rainfall and snowfall amounts based on the characteristics of precipitation particles. The results show that the total winter precipitation for each year ranged from 101.9 to 399.6 mm. Rainfall ranged from 5.9 to 80.2 mm, accounting for 17.0% of the total precipitation, 95.6% of which occurred in December and March. Identifying the causes of inter-annual variation is a future challenge.

The time series findings of daily precipitation indicate that significant snowfall and rainfall events contributed significantly to total winter precipitation. Cases of a significant snowfall event on January 19–20, 2016 and a rainfall event on March 9, 2018 were examined in detail. The events occurred in rising temperatures associated with synoptic-scale disturbances. Snowfall occurred when temperatures were below freezing after warming, and rainfall occurred when temperatures were above freezing.

Temperatures during synoptic-scale disturbances are central to discriminating between snowfall and rainfall events. The conditions that determine whether temperatures will exceed the freezing point include the temperature distribution on a synoptic-scale; the

horizontal scale of the disturbance, which affects air temperatures associated with advection; and the location and route of passage of the disturbance.

Although determining whether the location of disturbances that pass over Hokkaido will change with seasonal progression, and whether the location and passage of disturbances will be affected by global warming, lie beyond the scope of this study, these questions are relevant to whether precipitation in Rikubetsu will be dominated by snowfall or rainfall in the future. These studies are the subject of future work.

Japan has snowfall only in winter, and in terms of areas with snowfall, it is located at the southernmost tip of the Arctic snowfall region. It is possible that Japan may be removed from the Arctic snowfall region as a result of global warming. Rikubetsu is the coldest region in Japan, so it may be the last remaining snowfall area in Japan. This study summarized the current status on snowfall in such a region.

## Acknowledgements

The observation was conducted as part of a scientific project of National Institute of Polar Research (NIPR) through Project Research No. KP-302. This study was supported by JAXA's (The Japan Aerospace Exploration Agency) EORA3 (The 3rd Research Announcement on the Earth Observations) program.

## References

- Gunn, R. and G. D. Kinzer (1949): The terminal velocity of fall for water droplets in stagnant air. *J. Atmos. Sci.*, **6**(4), 243–248. [https://doi.org/10.1175/1520-0469\(1949\)006<0243:TTVOFF>2.0.CO;2](https://doi.org/10.1175/1520-0469(1949)006<0243:TTVOFF>2.0.CO;2).
- Hirasawa, N. and H. Konishi (2023): Diurnal variation in precipitation and cloud formation during winter in Rikubetsu, inland Hokkaido, northern Japan. *Okhotsk Sea and Polar Oceans Research*, **7**, 30-35. [doi.org/10.57287/ospor.7.30](https://doi.org/10.57287/ospor.7.30)
- Hirasawa, N., H. Konishi, K. Nishimura, C. Genthon and project group of Japan Meteorological Agency (2018): SPICE site report: Rikubetsu, Japan. WMO Solid Precipitation Intercomparison Experiment (SPICE), *Instruments and Observing Methods*, **131**, Annex 8.3, December 2018.
- Kawase, H., S. Fukui and 6 co-authors (2023): Historical regional climate changes in Japan in winter as assessed by a 5-km regional climate model with a land surface process. *Prog. Earth Planet. Sci.*, **10**(1), 7. <https://doi.org/10.1186/s40645-023-00536-4>
- Kawase, H., A. Murata and 7 co-authors (2021): Regional characteristics of future changes in snowfall in Japan under RCP2.6 and RCP8.5 scenarios. *SOLA*, **17**, 1–7, [doi:10.2151/sola.2021-001](https://doi.org/10.2151/sola.2021-001)
- McCrystall, M. R., J. Stroeve, M. Serreze, B. C. Forbes, and J. A. Screen (2021): New climate models reveal faster and larger increases in Arctic precipitation than previously projected. *Nat. Commun.*, **12**(1), 6765. <https://doi.org/10.1038/s41467-021-27031-y>
- Nayak, S., and T. Takemi (2020): Clausius-Clapeyron scaling of extremely heavy precipitations: Case studies of the July 2017 and July 2018 heavy rainfall events over Japan. *J. Meteor. Soc. Japan*, **98**, 1147–1162, [doi:10.2151/jmsj.2020-058](https://doi.org/10.2151/jmsj.2020-058).
- Nitu, R., and 42 co-authors (2018): WMO Solid Precipitation

- Intercomparison Experiment (SPICE). *Instruments and Observing Methods*, **131**. <https://library.wmo.int/opac/>
- Pickering, B. S., R. R. Neely III and D. Harrison (2019): The Disdrometer Verification Network (DiVeN): a UK network of laser precipitation instruments, *Atmos. Meas. Tech.*, **12**, 5845–5861, <https://doi.org/10.5194/amt-12-5845-2019>.
- Sorai, T., H. Hamada, T. Kameda, and S. Takahashi (2016): Rikubetsu, the coldest town in Japan: according to the meteorological data by Japan Meteorological Agency from 2007 to 2016 in winter seasons. *Tenki*, **63**, 879–887. (in Japanese)
- Takahashi, H. G. (2021): Long-term trends in snowfall characteristics and extremes in Japan from 1961 to 2012. *Int. J. Clim.*, **41(4)**, 2316–2329. <https://doi.org/10.1002/joc.6960>
- Trenberth, K. E., A. Dai, R. M. Rasmussen, and D. B. Parsons, (2003): The Changing Character of Precipitation. *Bull. Amer. Meteor. Soc.*, **84(9)**, 1205–1218. <https://doi.org/10.1175/BAMS-84-9-1205>.
- Vihma, T., J. Screen and 6 co-authors (2016): The atmospheric role in the Arctic water cycle: A review on processes, past and future changes, and their impacts. *J. Geophys. Res. Biogeosci.*, **121(3)**, 586–620. <https://doi.org/10.1002/2015JG003132>

## Summary in Japanese

和文要約

### 北海道内陸部の陸別における冬季の降雪量と降雨量の季節内変動と年々変動

平沢尚彦<sup>1,2</sup>, 小西啓之<sup>3</sup>

<sup>1</sup> 国立極地研究所, <sup>2</sup> 総合研究大学院大学, <sup>3</sup> 大阪教育大学

地球温暖化によって降水量は増加し、降雨の比率が増加する可能性がある。これまで世界的にも降雪と降雨を分離した継続的観測はほとんど行われておらず、降雪と降雨の比率の今後の変化を示すことは難しい。最近世界中で利用され始めた低価格のディズドロメータは降水粒子の特性に基づいて降雪と降雨を別々に記録できる。本研究は、現在の気候に関する情報の一つとして、北海道陸別における2012-13年から2022-23年の冬期の降雪量と降雨量をディズドロメータの観測値を用いて調べた。それは北極降雪圏の最南端の一地域の現状を表す。その結果、各年の冬期の総降水量は101.9~399.6 mm、降雨量は5.9~80.2 mmで総降水量の17%を占め、そのうちの96%は12月と3月に発生していた。降雨の占める割合は、それぞれ、1月と2月に2%、12月と3月に27%であった。顕著な降雪と降雨は冬期の総降水量に大きく寄与したが、それらは総観規模擾乱に伴って昇温とともに発生した。昇温後の気温が氷点下の時に降雪、氷点を上回った時に降雨となっていた。今後の気候変化において、総観規模擾乱時の気温が陸別の降雨量の鍵を握っていると考えられる。

Correspondence to: N. Hirasawa, [hira.n@nipr.ac.jp](mailto:hira.n@nipr.ac.jp)

Copyright ©2024 The Okhotsk Sea & Polar Oceans Research Association. All rights reserved.



# Intra-seasonal and interannual variations of sea ice along the Okhotsk coast of Hokkaido from the viewpoint of atmospheric circulation

Yuki ASAZUMA<sup>1</sup>, Masaya KURAMOCHI<sup>1</sup>, and Hiroaki UEDA<sup>2</sup>

<sup>1</sup> Graduate School of Science and Technology, University of Tsukuba, Tsukuba, Japan

<sup>2</sup> Faculty of Life and Environmental Sciences, University of Tsukuba, Tsukuba, Japan

(Received September 29, 2023; Revised manuscript accepted January 16, 2024)

## Abstract

In this study, we analyzed the intra-seasonal variations in sea ice along the Okhotsk coast of Hokkaido and clarified its relationship with atmospheric circulation fields based on observational data at Abashiri for 63 years (1958–2020). The results show that sub-weekly timescale variations are related to transient atmospheric disturbances that induce meridional winds and drive the sea ice near Hokkaido. When sea ice approaches the coast, atmospheric fields are marked by northerly winds to the rear of the developing extratropical cyclones that pass eastward near Japan. However, sea ice leaving the coast results from a southerly anomaly due to the weakened Siberian High and eastward-moving anticyclone. This study also investigated the interannual variations in sea ice along the coast of Hokkaido. During heavy sea-ice years, intensification of the Aleutian Low is discernible associated with northerly anomalies over the Okhotsk Sea and the enhancement of cold air intrusion toward Hokkaido. Simultaneously, diabatic cold air mass (CAM) genesis indicates that the accumulation of CAM near Hokkaido can be ascribed to an increase in the insulation effect due to the presence of sea ice. These findings provide the combined effect of the anomalous atmospheric fields and sea-ice insulation effect could be responsible for the significant negative correlation between air temperature and sea ice on the coast of Hokkaido.

**Keywords:** sea ice, Okhotsk Sea, Hokkaido, intra-seasonal variation, interannual variation

## 1. Introduction

The Okhotsk Sea (OS) is located in the western North Pacific and is characterized by seasonal sea ice. Climatologically, sea ice forms along the coast of Siberia because of the northwesterly winter winds. Sea ice drifts southward along the eastern coast of the Sakhalin Peninsula and reaches the coast of Hokkaido (COH) between January and March. Coastal sea ice near Hokkaido affects socio-economic activities, including sightseeing, around the Shiretoko World Heritage Site.

It is widely accepted that surface wind is one of the main factors that drives sea-ice motion, which is nearly parallel to the wind (Kimura and Wakatsuchi, 1999, 2000; Simizu *et al.*, 2014). Thus, many previous studies on sea-ice variability in the OS have focused on atmospheric circulation. It has been indicated that the intensity of the Aleutian Low accompanied by anomalous northerly winds over the OS is closely associated with the interannual variation in the Okhotsk sea-ice extent (Tachibana *et al.*, 1996; Yamazaki, 2000; Ueda *et al.*, 2023). Yamazaki (2000) and Ogi and Tachibana (2006) suggested a relationship between interannual sea ice variability and the Arctic Oscillation (AO; Thompson and Wallace, 1998)/North Atlantic Oscillation. Ueda *et al.* (2023) indicated that a wave train forced by tropical convective heating affected the Okhotsk sea-ice variation. The anomalous sea-ice extent

in the OS also affects the large-scale atmospheric circulation over the North Pacific through the supply/isolation of anomalous heat flux from the ocean surface to the atmosphere, which excites atmospheric Rossby waves (Honda *et al.*, 1999). On a daily to weekly time scale, Kamae *et al.* (2023) pointed out that the rapid reductions in sea-ice extent in the OS are linked to surface easterly winds over the OS associated with eastward-moving extratropical cyclones.

These studies focused on the variation in sea-ice extent over the entire OS. Coastal sea ice with thinner ice and lower sea-ice concentration (SIC), such as sea ice near the COH (Toyota *et al.*, 2022), is known to respond more strongly to atmospheric forcing as the response of sea ice to wind stress depends on ice thickness (Schevchenko *et al.*, 2004). It has been reported that the SIC in the northern to middle OS and along the COH varies in an opposite manner on daily-to-weekly (Kamae *et al.*, 2023) and year-to-year time scales (Aota *et al.*, 1988; Honda, 2007). On an intra-seasonal timescale, Aota *et al.* (1988) showed that rapid increases and decreases in sea ice along the COH correspond to the surface pressure gradient between Wakkanai (the northernmost city of Hokkaido) and Nemuro (the easternmost city of Hokkaido) associated with inshore and offshore winds. Toyota *et al.* (2022) indicated that variations in the first appearance/final disappearance

date are closely associated with variations in the Aleutian Low with meridional wind anomalies over the OS. It is also well known that sea ice along the COH is related not only to the meridional wind but also to the surface air temperature (SAT) near Hokkaido (Aota *et al.*, 1988; Takahashi *et al.*, 2011; Toyoda *et al.*, 2022).

Although previous studies have suggested the importance of meridional winds in sea ice variation along the COH, the daily-to-weekly wind variation relevant to large-scale atmospheric circulation has not yet been clarified. Therefore, the main objective of this study is to clarify the atmospheric circulation pattern that produces intra-seasonal variations in sea ice along the COH. Climatologically, the western North Pacific is characterized by a storm track due to its high lower-tropospheric baroclinicity (*e.g.* Chen *et al.*, 1991; Nakamura and Sampe, 2002). We hypothesize that the developing transient atmospheric disturbances induce the Wakkanai-Nemuro pressure gradient and meridional winds, as shown by Aota *et al.* (1988), which contribute to intra-seasonal variations in sea ice along the COH. Moreover, we discuss the interannual sea ice variability along the COH in comparison to its intra-seasonal variation.

## 2. Data

In this study, we used daily SIC data for 1958–2020 based on direct observations at Abashiri conducted by the Japan Meteorological Agency (JMA), which widely captures SIC variations along the COH on yearly and sub-weekly time scales (Aota *et al.*, 1988; Toyoda *et al.*, 2022). Moreover, the Abashiri Local Meteorological Observatory provides the SIC data for the longest period in comparison with that of the other meteorological observatories that face the OS such as Kitami-Esashi, Omu and Mombetsu. The data were obtained from visual observations at Abashiri at 9 a.m. within the range of 20 km from the Abashiri observatory and are indicated by 0–10, including locally formed ice up to 1. These data enabled us to analyze sea ice variations including the period before the start of satellite observations. Moreover, we used daily SIC data derived from the NOAA Optimum Interpolation Sea Surface Temperature V2 for 1981–2020 (Reynolds *et al.*, 2002) to confirm the SIC duration in the OS. Based on these daily SICs, we calculated the yearly-accumulated SIC (YA-SIC), which is often used as an index of interannual variation in sea ice along the COH (Aota *et al.*, 1988; Takahashi *et al.*, 2011; Toyoda *et al.*, 2022). The start and end dates of sea-ice existence at Abashiri for 1958–2020, provided by the JMA, were also used.

The atmospheric dataset used in this study was the Japanese 55-year Reanalysis (JRA-55; Kobayashi *et al.*, 2015) from 1958 to 2020. This study utilized the definition of cold air mass (CAM) based on a specific isentropic surface  $\theta_T$  (Iwasaki *et al.*, 2014), which is

a useful tool for diagnosing coldness and cold airflows. The amount of CAM is defined as

$$DP \equiv p_s - p(\theta_T), \quad (1)$$

where  $p_s$  is the surface pressure and  $p(\theta_T)$  the pressure on the  $\theta_T$  surface. The CAM conservation equation is as follows:

$$\frac{\partial}{\partial t} DP = -\nabla \cdot \int_{p(\theta_T)}^{p_s} \mathbf{v} dp + G(\theta_T), \quad (2)$$

The CAM amount changes results from horizontal convergence of CAM flux (**MF**) and the diabatic heating rate ( $G(\theta_T)$ ) which are defined as follows:

$$\mathbf{MF} = \int_{p(\theta_T)}^{p_s} \mathbf{v} dp, \quad (3)$$

and

$$G(\theta_T) = \left. \frac{\partial p}{\partial \theta} \dot{\theta} \right|_{\theta_T}, \quad (4)$$

where  $\mathbf{v} = (u, v)$  is the horizontal wind vector with the zonal wind  $u$  and the meridional wind  $v$ , and  $\dot{\theta}$  indicates the diabatic heating rate. The diabatic change rate (Eq. 4) is the source of the CAM (hereafter referred to as the CAM genesis/loss). The threshold potential temperature  $\theta_T$  is set to 280 K, following previous studies (*e.g.* Iwasaki *et al.*, 2014; Ueda *et al.*, 2023). SAT observational data at Abashiri, provided by the JMA, from 1958 to 2020 were used.

## 3. Climatology and intra-seasonal variations

### 3.1 Characteristics of sea ice along the COH

First, we examined the climatological sea-ice duration along the COH. Figure 1 shows the distribution of the climatological mean YA-SIC values. The YA-SIC east of Sakhalin exhibits larger values associated with sea ice drifting from the northern part of the OS to nearby Hokkaido due to the East Sakhalin Current (Simizu *et al.*, 2014). The YA-SIC was larger in the eastern part of the

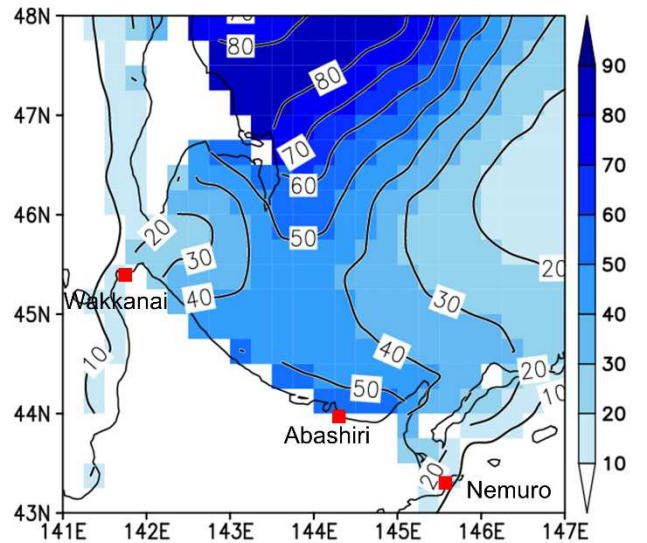


Fig. 1 Climatological mean YA-SIC from 1980/81 to 2019/20 (December–May) based on NOAA OISST V2.

Table 1. Monthly correlation coefficients of monthly SIC at Abashiri.

	start dates	DEC–JAN	FEB	MAR	APR–MAY	YA-SIC
start dates	1.000	−0.667	−0.490	−0.239	0.025	−0.488
DEC–JAN		1.000	0.574	0.216	0.033	0.623
FEB			1.000	0.563	0.272	0.840
MAR				1.000	0.693	0.856
APR–MAY					1.000	0.613
YA-SIC						1.000

COH than in the northern part. The locally long and high SIC is induced by the dam effect in the Shiretoko Peninsula (Aota *et al.*, 1988; Takahashi *et al.*, 2011).

We also analyzed the persistence of sea ice from winter to the following spring. Table 1 shows the monthly correlation coefficients of SIC at Abashiri. As for the month-wise correlation, positive correlations were salient, indicating the persistence of SIC in the COH for approximately two months. Moreover, the correlation between the start date and monthly SIC was negative from December to March, indicating that the earlier the first date, the larger the monthly SIC. These characteristics are consistent with the persistence of sea ice throughout the OS (Yamazaki, 2000; Ueda *et al.*, 2023).

### 3.2 Intra-seasonal variations of COH sea ice

Figure 2 shows the daily variation in SIC during 2019/20 winter as a sample. Sea ice along the COH exhibited large and rapid intra-seasonal variability. In this subsection, a composite analysis is performed on the day when sea ice rapidly approaches or leaves the COH during the sea ice season [hereafter referred to as approaching day (AD) and leaving day (LD), respectively]. Rapid variations are regarded as periods in which the SIC at Abashiri increases or decreases by five or more within three days. In this period, ADs and LDs were defined as the first days when the SIC

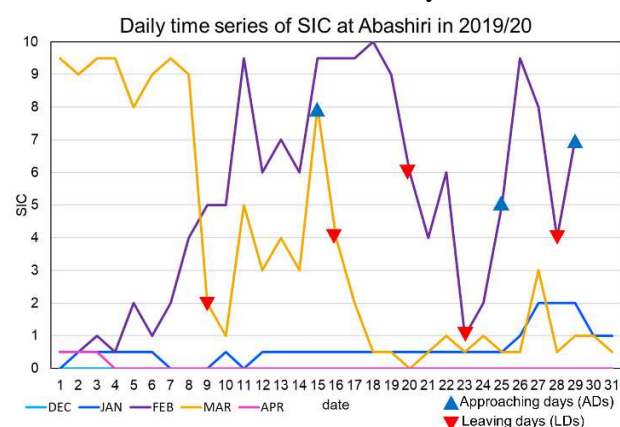


Fig. 2 Time series of daily SIC in 2019/20 from December to May. Triangles and inverted triangles denote approaching days (ADs) and leaving days (LDs), respectively.

increased and decreased by three or more, respectively. For the setting of the criteria, we have visually checked the daily variation of SIC and its spatial distribution for all years. We extracted 280 and 283 days for the ADs and LDs, respectively, during the 63-yr analysis period.

Figure 3 shows the temporal evolution of the anomalous atmospheric circulation [*i.e.* sea level pressure (SLP), surface horizontal wind, and geopotential height at 250 hPa (Z250)] around AD (day 0). Composite anomalies were defined as departures from the climatological mean for the corresponding calendar days. On day −2, an anomalous cyclone, located nearby Japan, moves eastward with developing and is accompanied with northerly winds nearby Hokkaido from day −1 to day 0. The horizontal SLP gradient around the cyclone was weak before the cyclone passed across Hokkaido but it strengthened after the center reached east of Hokkaido and subsequent intensification of the northerly wind, which induced a significant northerly wind in the rear part of the cyclone. The negative anomaly of Z250 was also salient to the west of the surface cyclone, and the upper-level trough gradually approached the surface cyclone while the cyclone moved eastward over the OS. This feature is indicative of a typical vertical structure in the developing stage relevant to baroclinic instability. The coupling of the surface cyclone and upper-level trough is often observed over the western North Pacific during winter and plays an important role in (explosively) developing cyclones, such as the Sea of Japan cyclone and the south coast cyclone (Nitta and Yamamoto, 1973; Takayabu, 1991). Using a numerical model, Kawano and Kawamura (2018) revealed that the anomalous sea-ice extent in the OS enhances the northerly winds to the rear of the cyclone. Considering their findings, it is implicated that the presence of a two-way interaction between transient cyclones and sea ice.

Figure 4 shows the temporal evolution of the anomalous atmospheric circulation around the LD. From day −2 to day 0, negative and positive SLP anomaly locates over the Eurasian continent toward the west of Japan and in the east of Japan, respectively, which produce a westward pressure gradient force and geostrophically balance the southerly wind anomaly nearby Hokkaido. The positive Z250 anomaly was also discernable west of the surface anticyclone. Moreover,

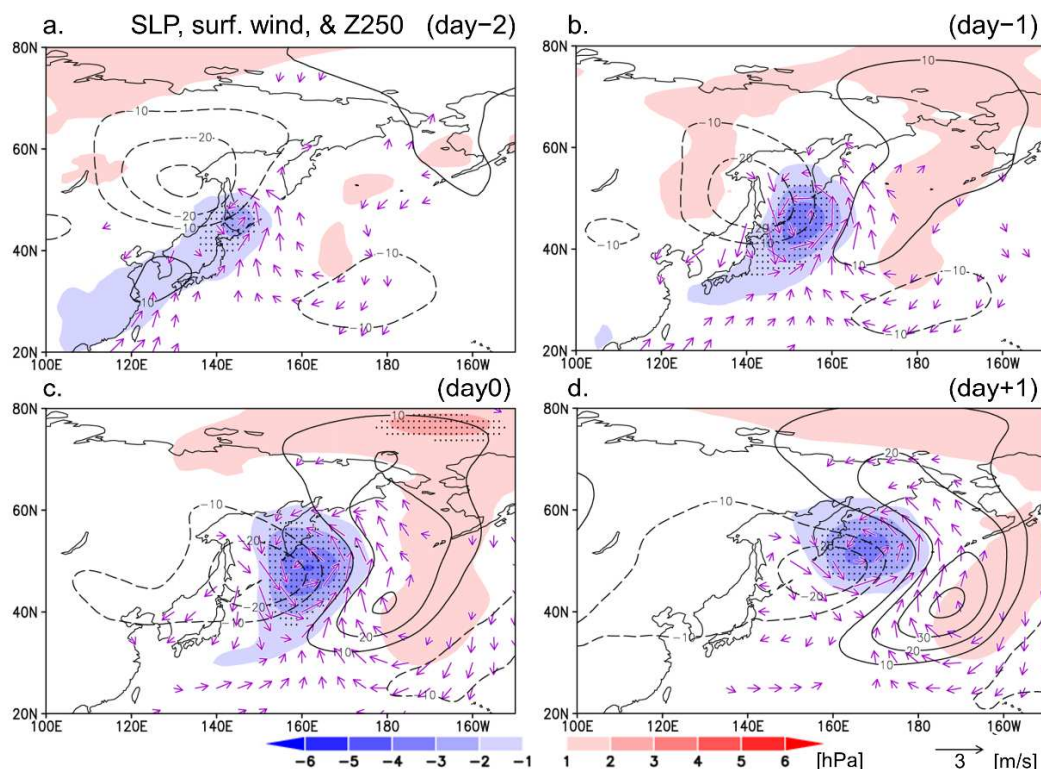


Fig. 3 Lagged composite anomalies for the days relative to the approaching days (ADs; day 0) in which shading denotes SLP (hPa), contours denote Z250 (interval: 10 m), and vectors denote the surface horizontal winds ( $\text{m s}^{-1}$ ). The vectors less than  $0.5 \text{ m s}^{-1}$  were omitted. Stippling denotes the SLP anomalies significant at a 95% confidence level.

the upper-level ridge gradually approached the surface anticyclone, while the anticyclone moved eastward. Prior to the LD (day  $-2$ ), the negative SLP anomaly indicates a weakening of the Siberian High together with the negative Z250 anomaly over northern Siberia. This feature is consistent with the anomalous vertical structure that contributes to the development and weakening of the Siberian High, as shown by Takaya and Nakamura (2005). In general, the attenuated Siberian High was responsible for the warmer climate over the Far East. Therefore, it is conceivable that the sea ice leaving the Okhotsk coast is also caused by in situ sea ice melting as well as southerly wind-induced ice drift.

#### 4. Interannual variations of sea ice along the COH

The previous section demonstrated the importance of transient atmospheric disturbances on sub-weekly scale sea ice variations in the COH. However, the correlation between the AD/LD frequency during the sea ice season and the interannual variability of the YA-SIC was weak ( $r = 0.18/0.17$ ). This suggests that intra-seasonal and interannual variations are controlled by different mechanisms.

A composite analysis was performed based on the YA-SIC index at Abashiri, which represents the year-to-year variability of sea ice along the COH. Figure 5 shows the year-to-year variations in YA-SIC at Abashiri from 1958 to 2020. The 1958 YA-SIC included SIC in December

1957. The heavy sea-ice years are defined as YA-SIC exceeding 1 standard deviation and light sea ice years are defined as that below  $-1$  standard deviation compared with the climatology. The standard deviation of the YA-SIC was 179.36 for 1958–2020. The standard deviation is widely adopted as the threshold to analyze interannual climate variations (*e.g.* Ueda *et al.*, 2023). On the basis of these criteria, 12 years (1961, 1963, 1964, 1965, 1970, 1977, 1978, 1979, 1981, 1984, 1986, 2003) are defined as the heavy sea-ice years. Likewise, 11 years (1989, 1990, 1991, 1992, 2004, 2006, 2007, 2009, 2010, 2016, 2020) are picked as the light sea-ice years. Notably, all heavy sea-ice years occurred before 2003, whereas seven of the 11 light sea-ice years occurred after 2003. Moreover, the YA-SIC at Abashiri clearly showed significant long-term decreasing trends ( $-65.12/\text{decade}$ ), implicating the influence of anthropogenic global warming. Composite maps were then constructed based on the January–March atmospheric circulation fields as the climatological start and end dates of the sea-ice existence at Abashiri for 1958–2020 were January 18 and April 9, respectively. The composite anomaly fields represent the deviations from the 63-yr climatology for January to March.

Figure 6 depicts the spatial distribution of YA-SIC anomalies. Note that the anomalies were computed for the heavy and light sea-ice years after 1980, owing to the data variable period. The SIC in the southern part of the

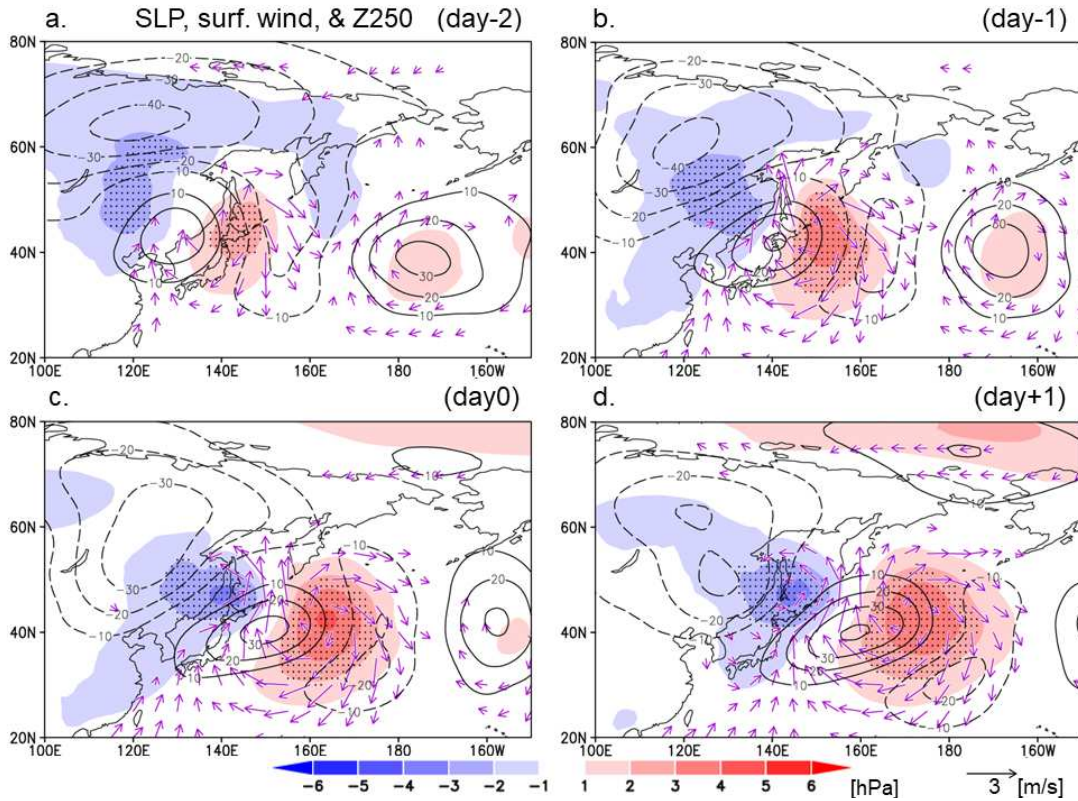


Fig. 4 Same as Fig. 3, but for the leaving days (LDs).

OS shows similar variations to the SIC along the COH. Interestingly, the YA-SIC in the heavy sea-ice year (Fig. 6a) shows a positive anomaly over the southern OS and a negative anomaly in the northern OS, which is consistent with the results of previous studies addressing sea ice before 1989 (Aota *et al.*, 1988; Honda, 2007). However, the YA-SIC in the light sea-ice year (Fig. 6b) showed a negative anomaly over the entire OS.

Figure 7 shows the composite anomalies of atmospheric circulations near the ground during years with heavy and light sea ice. For the heavy sea-ice years

(Fig. 7a), the intensification of the Aleutian Low, together with the anomalous northerly over the OS, is significant. This situation may be favorable for sea ice approaching the COH. The converse was true for light sea-ice years (Fig. 7b). Moreover, we did not find a significant anomaly in the Siberian High, which differs from the LD results. These results indicate that the intensity of the stationary Aleutian Low influences the interannual variability of sea ice along the COH as well as that of the entire OS (Yamazaki, 2000; Ueda *et al.*, 2023). However, if we take a close look at the anomalous

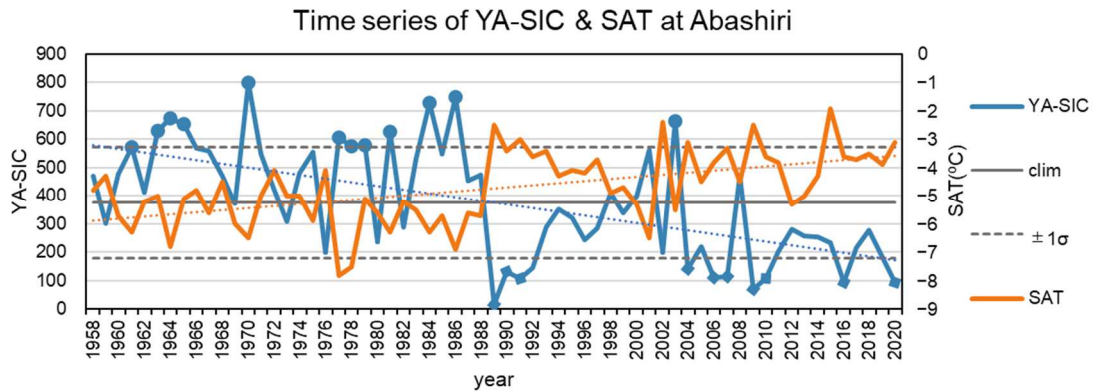


Fig. 5 Time series of Interannual variations of YA-SIC (blue) and SAT (orange) at Abashiri in from 1958 to 2020. Dotted lines indicate their linear trends by the corresponding color. Horizontal solid and dashed lines denote the climatological mean and 1 standard deviation of YA-SIC. SAT was averaged from January–March. Filled circles and diamonds denote the extracted heavy and light sea-ice years, respectively, in this study.

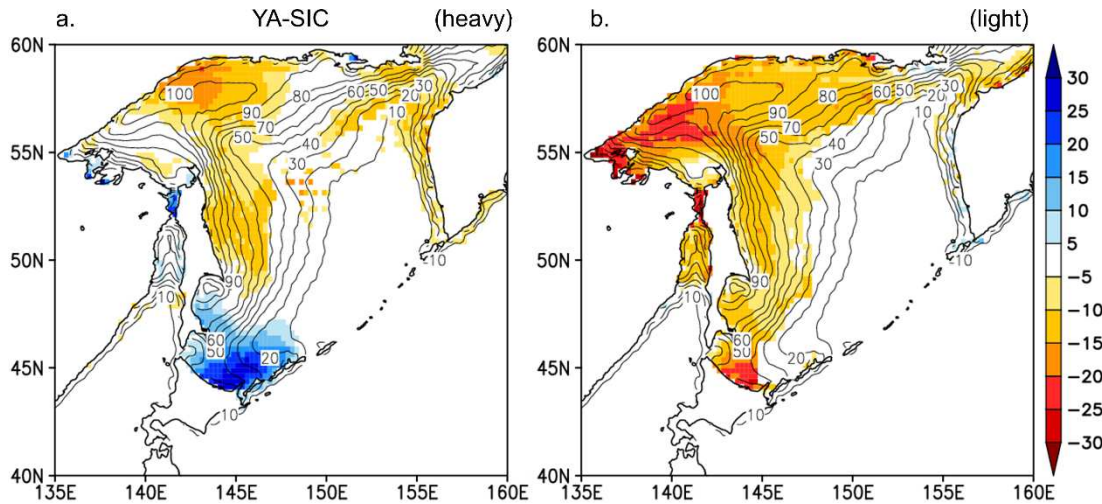


Fig. 6 Composite anomalies of YA-SIC (shading) in (a) heavy and (b) light sea ice years based on NOAA OISST V2. Contours indicate climatological YA-SIC in 1982–2020.

circulation fields in comparison with those in Ueda *et al.* (2023), there were local differences between the sea-ice variation in the COH and the entire OS. As for the wind direction, the anomalies relevant to the sea ice along the COH exhibited northeasterly (southwesterly) in the heavy (light) years (Fig. 7), whereas those in the entire OS were westerly (easterly) in its heavy (light) years (Ueda *et al.*, 2023). These differences are consistent with the locality of the SLP anomalies. The northeast-southwest direction of the wind variation is more effective for the sea ice approaching/leaving the COH and subsequent interannual variability.

It is widely accepted that sea ice along the COH is closely related to the local air temperature (Fig. 5; Aota *et al.*, 1988; Takahashi *et al.*, 2011). The correlation coefficient of YA-SIC at Abashiri against the mean air temperature at Abashiri in January–March was  $-0.81$ . We diagnosed the formation processes of the relationship between SAT and sea ice using the CAM. The local

CAM and SAT are highly correlated (Abdillah *et al.* 2018), and the CAM has an advantage in assessing the diabatic change in coldness (Eq. 2). Figures 8a and 8b show the composite anomalies of the CAM amounts and flux. In heavy sea-ice years (Fig. 8a), the CAM amount was significantly larger than normal near Hokkaido. The southwestward CAM flux anomaly from Alaska to the OS is consistent with the anomalous winds based on the effects of the intensification of the Aleutian Low, which indicates that the intensification of the Aleutian Low promotes the enhancement of cold air intrusion toward Hokkaido. In addition, the positive CAM genesis anomaly near COH was significant (Fig. 8c). This anomaly indicates the crucial role of an increase in the heat insulation effect (Martin *et al.*, 1998; Nihashi *et al.*, 2009) along the COH in the accumulation of CAM. In other words, the sea-ice insulation effects during heavy sea-ice years created an obstacle for heat gain to the atmosphere from the relatively warmer ocean, which

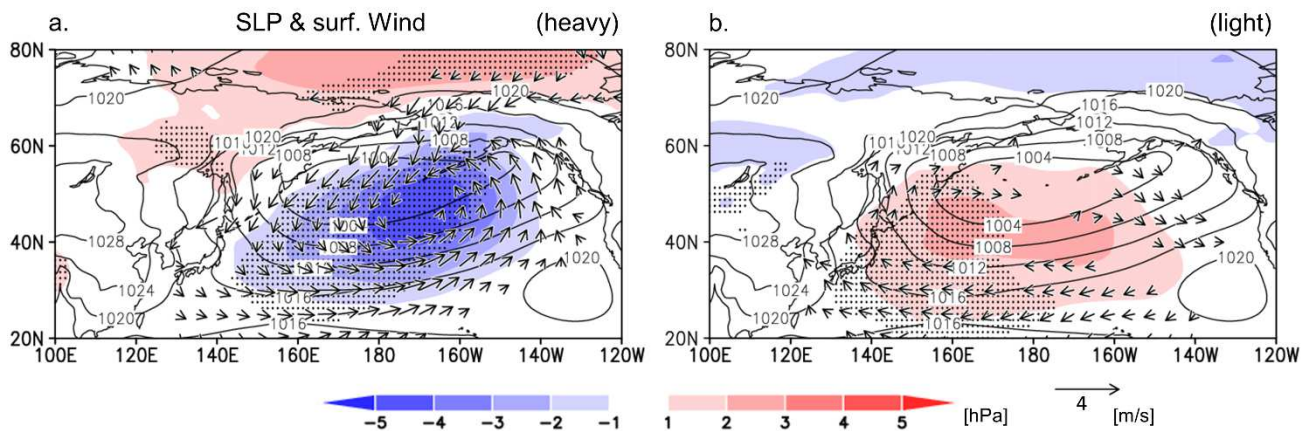


Fig. 7 (a) Composite anomalies in the heavy sea ice years of SLP (shading; hPa) and surface horizontal winds (vectors;  $\text{m s}^{-1}$ ). The vectors less than  $0.5 \text{ m s}^{-1}$  were omitted. Stippling denotes the SLP anomalies significant at a 95% confidence level. Contours denote January–March mean of the climatological SLP (interval: 4 hPa). (b) Same as (a), but for the light sea-ice years.

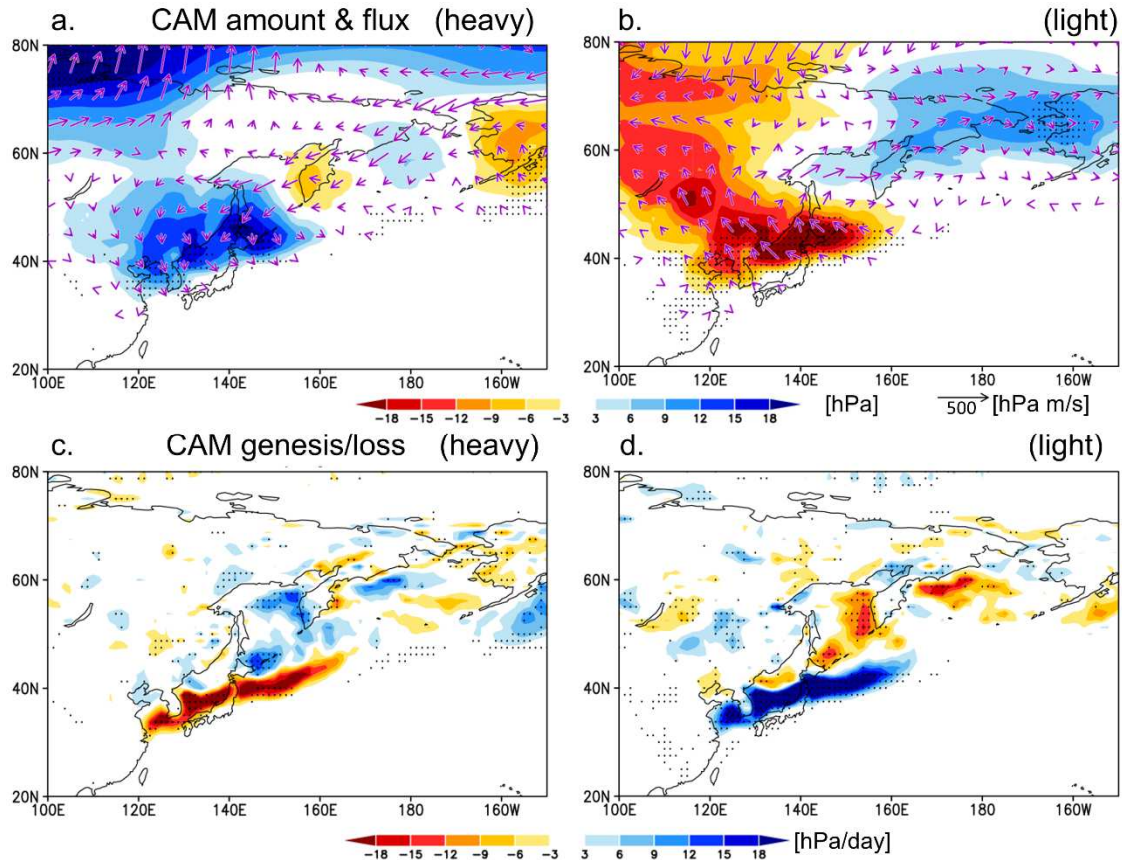


Fig. 8 (a) Composite anomalies in the heavy sea-ice years of CAM amount (shading; hPa) and CAM flux (vectors; hPa m s<sup>-1</sup>) below 280 K. Stippling denotes the CAM amount anomalies significant at a 95% confidence level. (b) Same as (a), but for the light sea-ice years. (c) Composite anomalies in the heavy sea-ice years of the CAM genesis/loss (shading; hPa day<sup>-1</sup>) below 280 K. Stippling denotes the CAM genesis/loss anomalies significant at a 95% confidence level. (d) Same as (c), but for the light sea-ice years.

would have contributed to the prominent cold anomalies in the southern OS. As for the light sea ice years (Fig. 8b), the amount of CAM was significantly lower near Hokkaido and over the Sea of Japan, implicating that the sea ice along the COH tends to melt easily. The CAM flux exhibits an anomalous anticyclonic circulation over the OS, including the anomalous southeasterly across the COH toward the Sea of Japan. The continental northwestward anomalies of CAM flux indicate a decrease in cold air outbreaks from East Asia. The negative anomalies of CAM genesis over the eastern and southern OS were due to the decrease in sea ice for the light years (Fig. 8d).

## 5. Summary and conclusions

We investigated seasonal variations in sea ice along the COH based on the Abashiri SIC over the last 63 years (1958–2020). According to the findings of this study, the intra-seasonal variation in sea ice along the COH is accompanied by meridional wind anomalies due to transient atmospheric disturbances. Sea ice approaching the coast results from northerly winds to the rear of a developing extratropical cyclone that passes eastward

near Japan. The cyclones detected in the present study can be ascribed to local depressions, such as the Sea of Japan cyclone or the south coast cyclone. In contrast, sea ice leaving the coast was dominated by a southerly anomaly owing to the weakened Siberian High and eastward-moving anticyclone. The weakening of the Siberian High was accompanied by a negative Z250 anomaly over northern Siberia, which resulted in mild weather conditions over the Far East. This study revealed the importance of atmospheric baroclinic waves on sub-weekly timescale sea-ice variations in the COH.

We also analyzed the interannual variability in sea ice along the COH. Heavy sea-ice years are characterized by the deepening of the Aleutian Low, which is accompanied by northeasterly winds and southward CAM flux anomalies toward Hokkaido. The composite anomaly of CAM genesis shows a significant positive anomaly near the COH, which implicates that the accumulation of CAM near Hokkaido is ascribed to an increase of the insulation effect due to the presence of sea ice. In contrast, the light sea-ice years displayed a weakening of the Aleutian Low and a decrease in diabatic CAM genesis. Thus, it is suggested that the

insulation effect caused by the presence of sea ice is responsible for the negative correlation between SAT and sea ice in Hokkaido. Simultaneously, the fluctuation in the Aleutian Low brings cold air and sea ice toward the COH. A deeper understanding of the atmospheric fields associated with sea-ice movement will improve prediction on a corresponding timescale and help interpret the responses of sea ice in the COH to climate change.

The YA-SIC at Abashiri clearly shows significant long-term decreasing trends together with increasing SAT trends (Fig. 5), in association with global warming. Recently, Tamura and Sato (2023) showed that the significantly increasing SAT trend over Japan, especially for days when cold air advection from the OS dominates, is associated with the retreat of OS sea ice. Our results on the interannual relationship between SAT and sea ice along the COH are consistent with their findings regarding the global warming trend. Therefore, it is essential to specify the process of decreasing sea-ice trends along the COH. As several time-scale variations in sea ice and the atmosphere include their interactions, further studies based on sensitivity experiments using numerical models are required to clarify causal relationship.

### Acknowledgments

SIC observation data were provided by the JMA. The authors acknowledge Drs. Humio Mitsudera (Hokkaido University), Takahiro Toyoda (Meteorological Research Institute) and Takenobu Toyota (Hokkaido University) for providing helpful information on the sea ice along the COH. We thank Dr. Tatsuro Karaki (University of Tsukuba) for fruitful discussions on sea-ice variation from the viewpoint of the ocean. We also thank Ms. Hitomi Yoshida (Okhotsk Garinko & Tower Co., Ltd.) for providing helpful local information. This study was supported by the Environment Research and Technology Development Fund (JPMEERF20214002) of the Environmental Restoration and Conservation Agency of Japan and the Japan Society for the Promotion of Science KAKENHI (21H00626 / 21H01154). The second author (MK) is supported by the JSPS Research Fellowship for Young Scientists.

### References

- Abdillah, M. R., Y. Kanno, and T. Iwasaki (2018): Strong linkage of El Niño–Southern Oscillation to the polar cold airmass in the Northern Hemisphere. *Geophys. Res. Lett.*, **45**, 5643–5652.
- Aota, M., M. Ishikawa, and E. Uematsu (1988): Variation in ice concentration off Hokkaido Island. *Low Temp. Sci., Ser. A*, **47**, 161–175.
- Chen, S. J., Y.-H. Kuo, P.-Z. Zhang, and Q.-F. Bai (1991): Synoptic climatology of cyclogenesis over East Asia, 1958–1987. *Mon. Wea. Rev.*, **119**, 1407–1418.
- Honda, M. (2007): Relationship between the Okhotsk sea ice and atmospheric field. *Kishou Kenkyu Note*, **214**, 63–73 (in Japanese).
- Honda, M., K. Yamazaki, H. Nakamura, and K. Takeuchi (1999): Dynamic and thermodynamic characteristics of atmospheric response to anomalous sea-ice extent in the Sea of Okhotsk. *J. Climate*, **12**, 3347–3358.
- Iwasaki, T., T. Shoji, Y. Kanno, M. Sawada, M. Ujiie, and K. Takaya (2014): Isentropic analysis of polar cold airmass streams in the northern hemispheric winter. *J. Atmos. Sci.*, **71**, 2230–2243.
- Kamae, Y., H. Ueda, T. Inoue, and H. Mitsudera (2023): Atmospheric circulations associated with sea-ice reduction events in the Okhotsk Sea. *J. Meteor. Soc. Japan*, **101**, 125–137.
- Kawano, T., and R. Kawamura (2018): Influence of Okhotsk sea ice distribution on a snowstorm associated with an explosive cyclone in Hokkaido, Japan. *SOLA*, **14**, 1–5.
- Kimura, N., and M. Wakatsuchi (1999): Processes controlling the advance and retreat of sea ice in the Sea of Okhotsk. *J. Geophys. Res.*, **104**, 11137–11150.
- Kobayashi, S., and 11 co-authors (2015): The JRA-55 reanalysis: General specifications and basic characteristics. *J. Meteor. Soc. Japan*, **93**, 5–48.
- Martin, S., R. Drucker, and K. Yamashita (1998): The production of ice and dense shelf water in the Okhotsk Sea polynyas. *J. Geophys. Res.*, **103**, 27771–27782.
- Nakamura, H., and T. Sampe (2002): Trapping of synoptic-scale disturbances into the North-Pacific subtropical jet core in midwinter. *Geophys. Res. Lett.*, **29**, doi: 10.1029/2002GL015535.
- Nitta, T., and J. Yamamoto (1974): On the observational characteristics of intermediate scale disturbances generated near Japan and the vicinity. *J. Meteor. Soc. Japan*, **52**, 11–31.
- Nihashi, S., K. I. Ohshima, T. Tamura, Y. Fukamachi, and S. Saitoh (2009): Thickness and production of sea ice in the Okhotsk Sea coastal polynyas from AMSR-E. *J. Geophys. Res.*, **114**, C10025.
- Ogi, M., and Y. Tachibana (2006): Influence of the annual Arctic Oscillation on the negative correlation between Okhotsk Sea ice and Amur River discharge. *Geophys. Res. Lett.*, **33**, L08709.
- Reynolds, R. W., N. A. Rayner, T. M. Smith, D. C. Stokes, and W. Wang (2002): An improved in situ and satellite SST analysis for climate. *J. Climate*, **15**, 1609–1625.
- Schevchenko, G. V., A. B. Rabinovich, and R. E. Thomson (2004): Sea-ice drift on the northeastern shelf of Sakhalin Island. *J. Phys. Oceanogr.*, **34**, 2470–2491.
- Simizu, D., K. I. Ohshima, J. Ono, Y. Fukamachi, and G. Mizuta (2014): What drives the southward drift of sea ice in the Sea of Okhotsk? *Prog. Oceanogr.*, **126**, 33–43.
- Tachibana, Y., M. Honda, and K. Takeuchi (1996): The abrupt decrease of the sea ice over the southern part of the Sea of Okhotsk in 1989 and its relation to the recent weakening of the Aleutian low. *J. Meteor. Soc. Japan*, **74**, 579–584.
- Takahashi, S., T. Kosugi, and H. Enomoto (2011): Sea-ice extent variation along the coast of Hokkaido, Japan: Earth's lowest-latitude occurrence of sea ice and its relation to changing climate. *Ann. Glaciol.*, **52**, 165–168.
- Takaya, K., and H. Nakamura (2005): Mechanisms of intraseasonal amplification of the cold Siberian high. *J. Atmos. Sci.*, **62**, 4423–4440.
- Takayabu, I. (1991): “Coupling development”: An efficient mechanism for the development of extratropical cyclones. *J. Meteor. Soc. Japan*, **69**, 609–628.
- Tamura, K., and T. Sato (2023): Localized strong warming and humidification over winter Japan tied to sea ice retreat. *Geophys. Res. Lett.*, **50**, e2023GL103522.
- Thompson, D. W. J., and J. M. Wallace (1998): The Arctic

- Oscillation signature in the wintertime geopotential height and temperature fields. *Geophys. Res. Lett.*, **25**, 1297–1300.
- Toyoda, T., Y. Kitamura, and R. Okada (2022): Sea ice variability along the Okhotsk coast of Hokkaido based on long-term JMA meteorological observatory data. *Okhotsk Sea and Polar Oceans Research*, **6**, 27–35.
- Toyota, T., N. Kimura, J. Nishioka, M. Ito, D. Nomura, and H. Mitsudera (2022): The interannual variability of sea ice area, thickness, and volume in the southern Sea of Okhotsk and its likely factors. *J. Geophys. Res.: Oceans*, **127**, e2022JC019069.
- Ueda, H., M. Kuramochi, and H. Mitsudera (2023): Interannual variations of sea-ice extent in the Okhotsk Sea—A pan-Okhotsk climate system perspective. *Atmosphere-Ocean*, **61**, 234–245.
- Yamazaki, K. (2000): Interaction between the wintertime atmospheric circulation and the variation in the sea ice extent of the Sea of Okhotsk. *Seppyo*, **62**, 345–354 (in Japanese).

## Summary in Japanese

和文要約

### オホーツク沿岸海氷の季節内・年々変動と 大気循環場

朝妻勇貴<sup>1</sup>, 倉持将也<sup>1</sup>, 植田宏昭<sup>2</sup>

<sup>1</sup>筑波大学理工情報生命学術院, <sup>2</sup>筑波大学生命環境系

北海道オホーツク沿岸海氷の季節内変動および年々変動と大気循環場の関係を調査した。事例合成解析の結果、北海道沿岸海氷の季節内変動は、日本付近を東進する移動性擾乱がもたらす南北風偏差が影響していることが示された。海氷の接岸時には、日本付近を発達しながら東進する低気圧の後面で北風偏差が見られ、海氷の移動と整合的である。一方、離岸時は、シベリア高気圧の弱化和移動性高気圧の通過に伴う南風偏差が顕著であった。沿岸海氷の年々変動についても調査した結果、多氷年ではアリューシャン低気圧の強化が確認された。同時にオホーツク海上で強化された北風に伴い、北海道への寒気流の強化が見られた。寒気質量の生成率偏差は、北海道沿岸で有意な正偏差を示し、海氷増加による海氷の断熱効果が北海道付近の寒気を増加させるように働く。北海道沿岸の海氷と気温の負の相関は、海氷の断熱効果と大気循環場の偏差の両者によりもたらされる事が示唆される。

Correspondence to: Y. ASAZUMA  
s2321113@u.tsukuba.ac.jp.

## Copyright

Copyright ©2024 The Okhotsk Sea & Polar Oceans Research Association. All rights reserved.



## Laboratory experiments on spray icing with urea-doped water using flat and cylindrical specimens

Toshihiro OZEKI<sup>1</sup>, Takatoshi MATSUZAWA<sup>2</sup>, Shingo NOMURA<sup>1</sup>,  
Satoru ADACHI<sup>3</sup>, Taiki TOKUDOME<sup>4</sup> and Akihisa KONNO<sup>4</sup>

<sup>1</sup>Hokkaido University of Education Sapporo, Sapporo, Japan

<sup>2</sup>National Maritime Research Institute, Mitaka, Japan

<sup>3</sup>Snow and Ice Research Center, National Institute of Earth Science and Disaster Resilience, Shinjo, Japan

<sup>4</sup>Kogakuin University, Hachioji, Japan

(Received November 17, 2023; Revised manuscript accepted January 26, 2024)

### Abstract

Urea-doped spray icing experiments were carried out on flat-plate and cylindrical specimens. The cylindrical specimens were tested at different diameters and the flat-plate was set directly facing the wind direction. Two wind speeds and three spray particle sizes were used. In the tests with diameters of 165 and 520 mm  $\Phi$ , approximately half of the impinging sprays froze; for the 60 mm  $\Phi$ , the icing rate was clearly greater than 50 %. This result suggests that the effect of diameter on the icing rate per impinging water varies between diameters of 60 mm  $\Phi$  and 165 mm  $\Phi$ . The amount of icing weight per unit time unit cross section increased with decreasing diameter. On the other hand, the increase in icing cross sectional area obtained from the graphical data analysis was greater for cylinders with a diameter of 520 mm and smaller for cylinders with a diameter of 165 mm. This result suggests that the horizontal cross-section of the icing growing on the specimen deviates from an elliptical shape as the diameter decreases. The icing rate of the flat plate is plotted as a function of its width, i.e. 1000 mm. The coefficient of determination for the logarithmic approximation is 0.77, which is in good agreement.

**Key words:** marine icing, spray icing, urea-doped water, wet growth, brine

### 1. Introduction

In recent years, the sea ice conditions of the Arctic Ocean have been changing annually and they will undergo further changes as global warming intensifies. As the open water area of the Arctic Sea route expands, the frequency of ships navigating that route will also increase. In the future, vessels with lower ice class and larger vessels will increasingly navigate. Marine icing will be an important factor in evaluating operational safety for vessels operating in weather and sea conditions where icing occurs.

Several researchers have simulated seawater spray icing growth. Makkonen (1987) developed a theoretical model of salt entrapment in spray ice. He assumed an analogy with sponginess of freshwater ice in wet growth. Lozowski *et al.* (2000) reviewed computer simulations of marine ice accretion and discussed the U. S. Coast Guard's Cutter Midgett model and a three-dimensional time-dependent vessel-icing model. Kulyakhtin and Tsarau (2014) applied a time-dependence model, MARICE, to the prediction of marine icing. MARICE calculated the turbulent airflow, trajectories of the droplets around the complete geometry of the structure, and heat transfer from the structure. Dehghani *et al.* (2017) and Dehghani *et al.* (2018) studied the water breakup phenomena of wave impact sea spray and

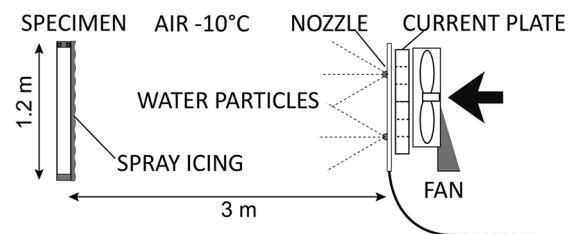


Fig. 1 A schematic view of experimental setting.

developed a three-dimensional model for calculating the movement of a cloud of wave-impact sea spray over a Medium-sized Fishing Vessel (MFV). The results of spray impingement on the front side of the superstructure showed that 70 % of the droplets are smaller than 2 mm and 30 % are between 2 and 4 mm.

Because the phenomenon of sea spray icing is complex and the growth of icing varies depending on the shape of the ship and its superstructure, the practical risk of icing has been evaluated based on a relatively simple empirical equation  $PR$  (Overland, 1990) as following,

$$PR = \frac{V_a(T_f - T_a)}{1 + 0.4(T_w - T_f)}, \quad (1)$$

where  $PR$  is the predictor relating to icing rate,  $T_f$  is freezing point of seawater [ $^{\circ}\text{C}$ ],  $T_a$  is air temperature [ $^{\circ}\text{C}$ ],  $T_w$  is sea temperature [ $^{\circ}\text{C}$ ],  $V_a$  is wind speed [ $\text{m s}^{-1}$ ]. The factor used to estimate the severity of potential spray icing is derived from a simplified heat balance of the icing surface, which do not consider the characteristics of individual ships or the availability of anti-icing measures.

Although the  $PR$  values are useful for evaluating the safety of icing during navigation, more information is needed to use them in ship design and operational planning. In this study, to obtain data that will contribute to the improvement of the  $PR$  equation, urea-doped spray icing experiment was conducted using a simple model of superstructure members.

## 2. Method of laboratory experiments

### 2.1 Equipment for spray icing experiments

The experimental apparatus (Fig. 1) was set up on an ice tank (20 m in length  $\times$  6 m in width  $\times$  1.8 m in depth) at the Technical Research Center of Japan Marine United Inc. The use of salt water is not permitted in this facility. The model ice for the ice tank test is made with urea-doped water so that brine is contained inside the ice. Therefore, we studied the icing characteristics of urea-doped water droplet icing including brine using a simple-shaped specimen.

Two fan-shaped nozzles (VE115-31 or VE115-59, Ikeuchi) and four fan-shaped nozzles (VP115-04, Ikeuchi) were installed on both sides of the fan, so that the sprayed water droplets were supplied to the specimen by the wind. The room temperature in the cold room was controlled at  $-10^{\circ}\text{C}$ , and urea water with a concentration of about 20 % was sprayed to grow brine-containing ice on the specimen.

In this study, PVC cylindrical specimens were tested at different diameters of 520 mm, 165 mm or 60 mm and

a height of 1.2 m (Fig. 2). Experiments on flat plate (1000 mm in length  $\times$  918 mm in height) were carried out as well. The flat-plate specimen, painted with blue marine paint, was fixed on a dolly facing the wind direction (Fig. 2). The distribution of wind velocity and droplet impact around the specimen was measured separately prior to each icing experiment. Spray particle counter (SPC-S7, Niigata Denki) was used to measure the particle size distribution of the droplets.

### 2.2 Visualization of brine structure in urea-doped spray ice using X-ray CT and MRI

Recently, X-ray computerized tomography (CT) has been used to measure the three-dimensional distribution of brine inside the sea ice nondestructively (Kawamura, 1988; Obbard *et al.*, 2009). Nuclear magnetic resonance (NMR) is compatible with brine and has been applied to the measurement of sea ice (Calaghan *et al.*, 1999). In addition, magnetic resonance imaging (MRI) can acquire contrasting images in brine and ice mixtures (Edelstein and Schulson, 1991; Eicken, 2000; Menzel *et al.*, 2000). Ozeki *et al.* (2005) measured the three-dimensional microstructure of sea-water spray ice using the MRI technique and confirmed the presence of such a channelized network of brine in natural sea-water spray ice samples (Fig. 3). In this study, X-ray CT and MRI system set up in a cold room was used to visualize the brine in sodium chloride ice.

We used a  $\mu\text{CT}$  35 system (SCANCO Medical) with a resolution of 1.75–72  $\mu\text{m}$  for the X-ray CT. Meanwhile MRI was performed using a yokeless magnet with a field strength of 1.04 T (Adachi *et al.* 2009). A three-dimensional single spin-echo (3D-SE) sequence (image matrix =  $256^3$ , voxel size =  $(100 \mu\text{m})^3$ ) was used for 3D high-resolution imaging. Each X-ray CT data and MRI data was analyzed using ImageJ that was an open source image processing software.



Fig. 2 Flat-plate and cylindrical specimens. Diameters of cylindrical specimens (left) are 520 mm, 165 mm, or 60 mm.

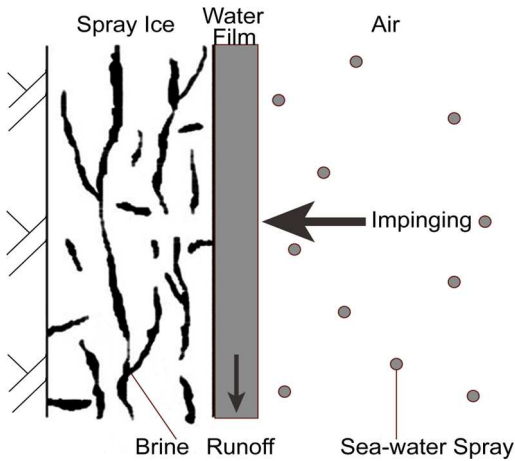


Fig. 3 A schematic vertical cross section of wet growth

Table 1. Specimen diameter and spray particle diameter (small droplet and very small droplet)

Diameter [mm]	VE115-31		VP115-04	
	10 m/s	7.5 m/s	10 m/s	7.5 m/s
60	#HS60	#MS60	#HV60	#MV60
165	#HS165	#MS165	#HV165	#MV165
520	#HS520	#MS520	#HV520	#MV520

Table 2. Nozzle model number for flat plate and corresponding cylindrical specimens.

Diameter [mm]	VE115-31	VE115-59
	10 m/s	10 m/s
Flat plate	#HSFlat	#HLFlat
60	#HS60	#HL60
165	#HS165	#HL165
520	#HS520	#HL520

### 3. Experimental results

#### 3.1 Observation of spray ice and brine distribution

The icing test on the cylindrical specimens was conducted eighteen times with different specimen diameters, wind speeds and spray particle sizes. The test conditions and test numbers for small particles (VE115-31) and very small particles (VP115-04) are given in Table 1. In this experiment, the wind speed was about 10 m/s (high speed) or 7.5 m/s (middle speed) near the center of the specimen. The spraying was supplied continuously. The tests were conducted for 30 minutes each (20 minutes for #HS520 test), and the ice weight were measured at the end of each test at each one sixth height. The icing test on the flat plate specimen was conducted two times with small particles (VE115-31) and large particles (VE115-59) for 30 minutes each, and the wind speed was about 10 m/s near the center of the specimen. The ice weight was measured at the end of each test at each one fourth height. The test conditions for the flat plate and corresponding cylindrical specimens test numbers are given in Table 2.

Spray particles impinging on the cylinder formed a

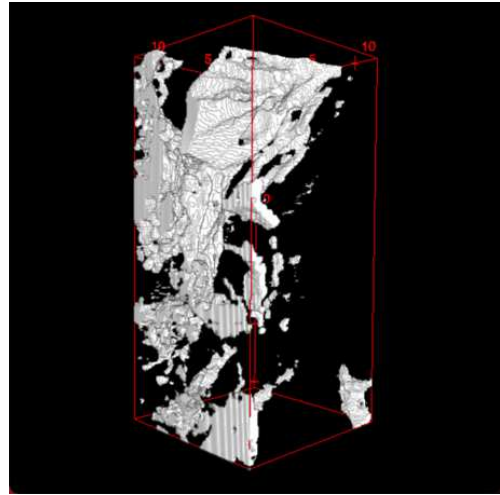


Fig. 4 Surface rendering of 3D X-ray image of brine distribution in spray ice created from 20% urea-doped spray water.

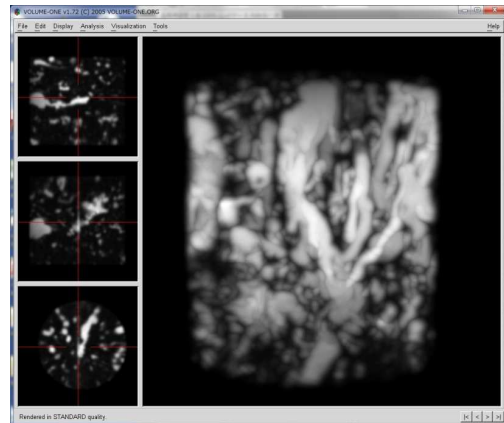


Fig. 5 3D MRI image of brine distribution in spray ice created from 30% sodium chloride spray water. (Ozeki *et al.*, 2013)

water film, and part of the water froze into spongy ice as it flowed down the PVC surface. In the early stage, part of the spray ice peeled off and slide down the surface as slush. The spray ice was spongy and had a milky white color. This is consistent with the characteristics of ice containing brine. Therefore, urea-doped spray ice was expected to contain a high amount of brine.

Fig. 4 shows a 3D X-ray image of brine network of spray ice created from 20% urea-doped water spray. We used surface rendering to visualize the brine pockets and channels. We have confirmed that the urea-doped spray ice contains a high amount of brine, the bright regions in the figure. A vertically converging drainage channel was observed in the brine distribution in the spray ice.

Fig. 5 shows 3D MRI image of brine distribution in spray ice created from 30% sodium chloride spray water. Since the NMR signal from the ice was negligible as compared to that from the brine, the brine drainage channels appeared as bright regions. Left windows shows 2D slices selected from the 3D image data. Brine

drainage channels appear vertically in the sodium chloride spray ice. Structurally, urea-doped spray ice and sodium chloride spray ice were found to have very similar brine channels.



Fig.6 Cross-section area of the spray ice. Left: a PVC cylinder of 520mm diameter (#MV520), Right: difference between the trimming area including the spray ice and the projected area of specimen.

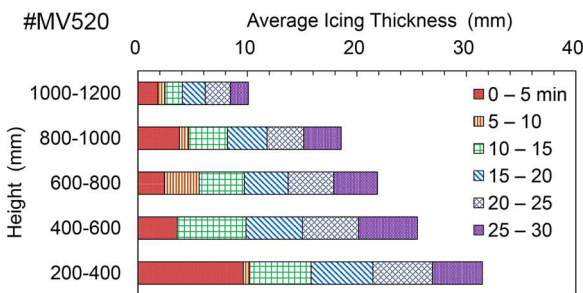


Fig. 7 Thickness of ice accretion every 5 minutes at every 20 cm height on a PVC cylinder of 520mm diameter (#MV520).

### 3.2. Graphic Data Processing

Projection area of ice accretion was obtained from graphic data set of each experiment (Fig. 6). In this study, the photographs were taken every minute from left side, and cropped to leave only the subjects that include ice accretion and the specimen. The cross-section area of the spray ice was obtained from the difference between the projected area of the trimming area including the spray ice and the projected area of specimen (Ozeki *et al.*, 2022).

Fig. 7 shows the cross-sectional area of ice accretion every 5 minutes at every 20 cm height in test #MV520, and converted to the average thickness of ice accretion every 5 minutes at each height. The projected area of 0-200 mm included ice piled up from the floor and was

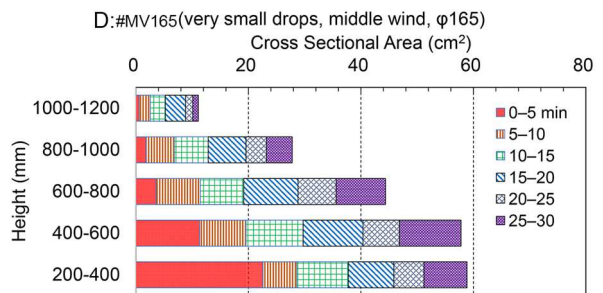
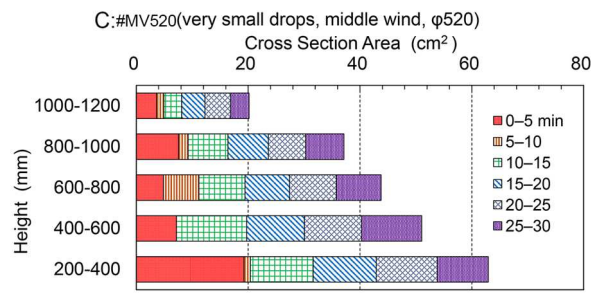
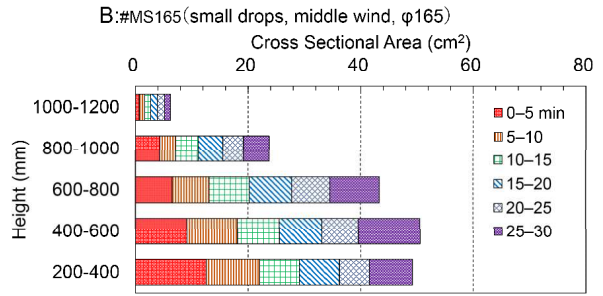
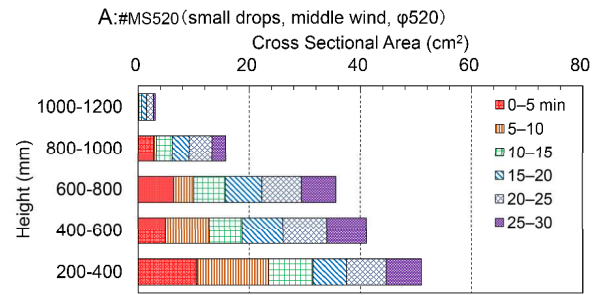


Fig. 8 Comparison of cross-sectional area of ice accretion every 5 minutes. A: #MS520, B: #MS165, C: #MV520, D: #MV165.

excluded from the analysis because it was difficult to separate ice accretion from ice on the floor. Focusing on the amount of growth during the first 5 minutes, the growth near the center of the cylinder (600-800 mm) was small. On the other hand, no growth was recorded at 400-600 mm in 5-10 min. This is because the sheet icing exfoliated and slide off. However, the growth became stable after that, and a distribution of thicker icing in the lower layers and thinner icing in the upper layers was formed after 30 minutes.

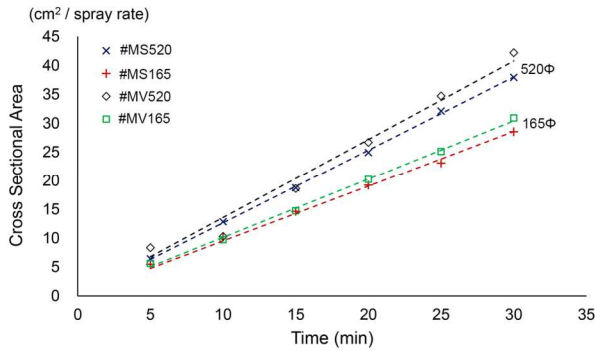


Fig. 9 Time series of cross-sectional area of ice accretion divided by the spray rate ( $\text{kg m}^{-2} \text{min}^{-1}$ ) every 5 minutes.

Fig. 8 shows four graphs of the cross-sectional area of ice accretion every 5 minutes for tests #MS520 (Fig. 8A), #MS165 (Fig. 8B), #MV520 (Fig. 8C), and #MV165 (Fig. 8D) at heights of every 20 cm. In this figure, the cross-sectional area ( $\text{cm}^2$ ), rather than the thickness of ice accretion (mm), was presented to comparison of each test. In the initial stage, there were differences in the vertical distribution of icing area depending on the diameter of the cylinder: for the specimens with 520 mm  $\Phi$  (#MS520, #MV520), the area decreased once at 400–600 mm, while for the specimens with 165 mm  $\Phi$  (#MS165, #MV165), the area monotonically increased toward the lower layers. However, after 30 minutes, the icing area in all specimens reached the distribution with thicker ice accretion in the lower layers and thinner ice accretion in the upper layers.

To compare the growth rate of icing on each test, the cross-sectional area of ice accretion was calculated every 5 minutes and divided by the spray rate ( $\text{kg m}^{-2} \text{min}^{-1}$ ) for each test was plotted in Fig. 9. In all times, the cross-section increased linearly with time. The increasing rate was greater for the 520 mm diameter cylinder and smaller for the 165 mm cylinder. For the same diameter, the increasing rate for very small particles (#MV) was slightly greater than that for small particles (#MS).

### 3.3 Spray icing ratio

Table 3 shows the amount of spray water impinging on the specimen per unit time and unit area ( $X$ ), and the amount of icing per unit time and unit area ( $Y$ ); the projected area of the side surface of the specimen was used to calculate per unit area. Since the wind speed, projected area, and droplet particle size of each test were different, a direct comparison of the above values does not reveal a relationship. Therefore, the spray icing ratio  $Y/X$ , which represents the freezing rate relative to the impinging urea-doped water, was calculated. In both experiments on cylindrical specimens with diameters of

Table 3. Amount of spray water impinging on the specimen and amount of icing

Specimen	X: Spray Rate [ $\text{kg m}^{-2} \text{min}^{-1}$ ]	Y: Ice Accretion [ $\text{kg m}^{-2} \text{min}^{-1}$ ]	Y/X
#HS520	1.04	0.50	0.48
#MS520	0.64	0.31	0.48
#HV520	0.86	0.46	0.53
#MV520	0.85	0.39	0.46
#HS165	1.37	0.65	0.47
#MS165	1.01	0.57	0.56
#HV165	1.11	0.71	0.64
#MV165	1.18	0.58	0.49
#HS60	1.51	1.11	0.74
#MS60	1.16	1.09	0.94
#HV60	1.57	1.13	0.72
#MV60	no data	0.97	N/A

Table 4. Spray icing ratio (icing/impinging spray water) on the flat plate specimen and cylindrical specimens. Wind speed 10 m/s in center of specimens.

Diameter	VE115-31	VE115-59
	Small particles	Large particles
Flat plate	0.34 (#HSFlat)	0.27 (#HLFlat)
60 mm $\Phi$	0.74 (#HS60)	1.01 (#HL60)
165 mm $\Phi$	0.47 (#HS165)	0.51 (#HL165)
520 mm $\Phi$	0.48 (#HS520)	N/A (#HL520)

165 mm  $\Phi$  and 520 mm  $\Phi$ , approximately half of the impinging spray was frozen under these conditions, and there was no significant difference in the amount of ice formed over the entire sample per unit area. On the other hand, in the cylindrical specimen with a diameter of 60 mm  $\Phi$ ,  $Y/X$  was clearly larger than 50%, and the small particle test at 7.5 m/s (#MS60) showed a high value of 94%.

Table 4 shows the spray icing ratio for the flat plate specimen. The spray icing ratio for cylindrical specimens under the same test conditions was shown in the table. The small particle nozzle VE115-31 and the larger particle nozzle VE115-59 were used, however the heavier particles fell before they reached the specimens, and SPC measurements showed little difference in the particle size distributions of the two nozzles. The flat plate tended to have lower icing ratio than the cylindrical specimens. Moreover, the distribution of spray icing was concentrated on the edges.

Fig. 10 shows the spray icing ratio as a function of cylindrical specimen diameter. The flat plate does not correspond to a diameter, thus is plotted for a width of 1000 mm, which corresponds to the width of the flat plate. The spray icing ratio tended to decrease as the diameter increased. The coefficient of determination for the logarithmic approximation is 0.77, which is in good agreement.

## 4. Discussion

The increasing rate of the spray icing cross-sectional area was greater for the 520 mm  $\Phi$  cylinder than for the

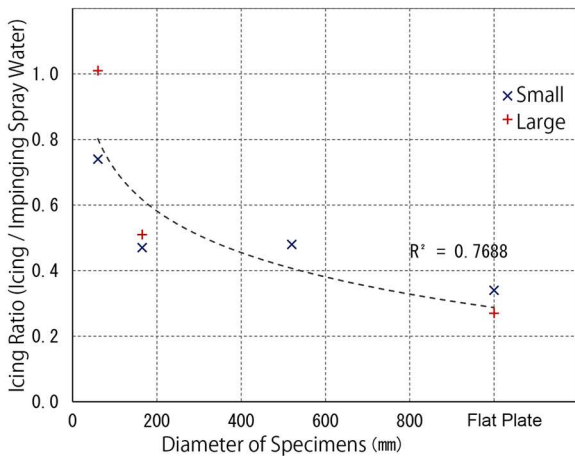


Fig. 10 Spray icing ratio as a function of the cylindrical specimen diameter. The flat plate is shown as equivalent to 1000 mm.

165mmΦ cylinder. On the other hand, the ratio of the amount of spray water impinging on the specimen (X) and the amount of spray icing (Y) was not significantly different between the spray icing ratio for 165 mmΦ and 520 mmΦ, with Y/X clearly larger for the 60 mmΦ cylinder. The difference between these two results is due to the difference in the horizontal cross-sectional shape of the spray icing.

Fig. 11 shows horizontal cross-sectional photographs of spray icing on 60 mm Φ, 165 mm Φ, and 520 mm Φ cylindrical specimens. The 520 mm Φ sample was thickest at the stagnation point on the windward front and became thinner toward the sides, while the 60 mm Φ sample had a shape where the edges protruded toward the sides. This is an expected result based on the trajectories of the streamlines and droplet particles. However, it is noteworthy that a change was observed between Φ165 mm and Φ60 mm. As a result, in the case of a thin cylinder, the icing grows significantly laterally, and its projected area become larger than the original projected area, which suggests that the amount of spray impinging the specimen was larger than the original.

### 5. Conclusion

Urea-doped spray icing experiment were conducted using a simple model of superstructure members. Twelve icing tests were conducted with different specimen diameters, wind speeds and spray particle sizes. After each test, ice weight and salinity were measured at each one-sixth height. In all tests of 165 mm Φ and 520mm Φ in diameter, approximately half of the impinging spray froze. On the other hand, in the tests using 60 mm Φ cylindrical specimen, frozen ratio was clearly larger than 50%. This result suggests that the effect of diameter on the icing rate per impinging water varies between diameters of 60 mm Φ and 165 mm Φ. The amount of icing weight per unit time unit cross section increased with decreasing diameter. On the other hand, the increase in icing cross sectional area obtained from the graphical data analysis was greater for cylinders with a diameter of 520 mm and smaller for cylinders with a diameter of 165 mm. This result suggests that the horizontal cross-section of the icing growing on the specimen deviates from an elliptical shape as the diameter decreases.

The experimental data will be useful for improving the PR equation by weighting the icing index according to the geometry of the object. Furthermore, as the development of icing is caused by the flight, collision, and freezing of wave spray particles, the icing index will be improved by estimating the trajectory of spray particles around the hull of a ship using CFD analysis.

### Acknowledgment

We wish to express our gratitude to S. Mizuno, N. Nakazato and A. Maeda of JMU Technical Research Center. This work was supported by ArCSII JPMXD1420318865.

### References

Adachi, S., T. Ozeki, R. Shigeki, S. Handa, K. Kose, T. Haishi, M. Aoki (2009): Development of a compact magnetic resonance imaging system for a cold room. *Rev. Sci. Instrum.*, **80**, Article 054701: doi.org/10.1063/1.3129362.



Fig. 11 Horizontal cross-sectional photographs of spray icing on 520 mm Φ, 165 mm Φ, and 60 mm Φ cylinders. The yellow reference line represents the icing contact point. The black double arrow line of 60 mm Φ represents the width of icing, which is larger than the diameter of the cylinder.

- Calaghan P.T., R. Dykstra, C.D. Eccles, T.G. Haskell and J.D. Seymour (1999): A nuclear magnetic resonance study of Antarctic sea ice brine diffusivity. *Cold Reg Sci Tech.*, **29**, 153–171: doi.org/10.1016/S0165-232X(99)00024-5.
- Dehghani, S.R., Y.S. Muzychka and G.F. Naterer (2017): Water breakup phenomena in wave-impact sea spray on a vessel. *Ocean Eng.*, **134**, 50-61: doi.org/10.1016/j.oceaneng.2017.02.013.
- Dehghani, S.R., G.F. Naterer and Y.S. Muzychka (2018): 3-D trajectory analysis of wave-impact sea spray over a marine vessel. *Cold Reg. Sci. Tech.*, **146**, 72-80: doi.org/10.1016/j.coldregions.2017.11.016.
- Eidelstein, W.A. and E.M. Schulson (1991): NMR imaging of salt-water ice. *J. Glaciol.*, **37**, 177–180: doi.org/10.3189/S0022143000042933.
- Eicken, H, C. Bock, R. Wittig, H. Miller and H.O. Poertner (2000): Magnetic resonance imaging of sea-ice pore fluids: methods and thermal evolution of pore microstructure. *Cold Reg. Sci. Technol.*; **31**: 207–225: doi.org/10.1016/S0165-232X(00)00016-1.
- Kawamura, T. (1988): Observations of the internal structure of sea ice by X ray computed tomography. *J. Geophys. Res.* **93**(C3), 2343–2350: doi:10.1029/jc093ic03p02343.
- Kulyakhtin, A. and A. Tsarau (2014): A time-dependent model of marine icing with application of computational fluid dynamics. *Cold Reg. Sci. Tech.*, 104-105, 33-44: doi.org/10.1016/j.coldregions.2014.05.001.
- Lozowski, E.P., K. Szilder and L. Makkonen (2000): Computer simulation of marine ice accretion. *Phil. Trans. R. Soc. Lond.*, **A358**, 2811–2845.
- Makkonen, L. (1987): Salinity and growth rate of ice formed by sea spray. *Cold Reg. Sci. Tech.*, **14**, 163–171.
- Menzel M.L., S. Han, S. Stapf and B. Blümich (2000): NMR characterization of the pore structure and anisotropic self-diffusion in salt water ice. *J. Magn. Reson.*, **143**: 376–381: doi.org/10.1006/jmre.1999.1999.
- Obbard, R.W., G. Troderman and I. Baker (2009): Imaging brine and air inclusions in sea ice using micro-X-ray computed tomography. *J. Glaciol.*, **55**, 1113–1115: doi.org/10.3189/002214309790794814
- Overland, J.E. (1990): Prediction of Vessel Icing for Near-Freezing Sea Temperature. *Weather and Forecasting*, **5**, 62-77.
- Ozeki, T., K. Kose, T. Haishi, S. Nakatsubo and Y. Matsuda (2005): Network images of drainage channels in sea spray icing by MR microscopy. *Mag. Res. Imag.*, **23**, 333-335.
- Ozeki, T., H. Shimoda, D. Wako, S. Adachi and T. Matsuzawa (2013): Laboratory experiments of saline water spray icing - Features of hydrophilic and hydrophobic pliable sheets. *Proc. Int. Workshop on Atmospheric Icing of Structure 2013*, 5pp.
- Ozeki, T., T. Matsuzawa, S. Adachi, T. Tokudome, T. Nunokawa, Y. Matsuda and A. Konno (2022): Laboratory experiment of spray icing using urea-doped water - Shape and amount of icing on cylindrical specimen with different diameters. *Proc. 36th Int. Symp. Okhotsk Sea and Polar Oceans*, 4pp.

## Summary in Japanese

和文要約

### 尿素水を用いた平板試験体及び円筒試験体への飛沫着氷実験

尾関俊浩<sup>1</sup>, 松沢孝俊<sup>2</sup>, 野村慎吾<sup>1</sup>, 安達聖<sup>3</sup>,  
徳留大樹<sup>4</sup>, 金野祥久<sup>4</sup>

<sup>1</sup>北海道教育大学札幌校, <sup>2</sup>海上技術安全研究所,  
<sup>3</sup>防災科研雪氷防災研究センター, <sup>4</sup>工学院大学

平板および円筒形の試験体を用いて、尿素を添加した飛沫着氷試験を行った。円筒試験体は直径 60, 165, 520 mm  $\Phi$  の 3 種類を用いた。平板試験体は風向に正対するように設置して着氷試験を行った。風速は 2 モード、噴霧粒子径は 3 種類を用いた。直径 165, 520 mm  $\Phi$  の試験体では、衝突した噴霧の約半分が凍結した。60 mm  $\Phi$  では着氷率が 50%より明らかに大きかった。一方、グラフデータ解析から得られた着氷断面積の増加量は、直径 520mm の円柱で大きく、直径 165mm の円柱で小さくなった。この結果は、試験体に成長した飛沫着氷の水平断面が、直径が小さくなるにつれて楕円形から逸脱することを示唆している。平板の着氷率をその幅にあたる 1000 mm に相当させてプロットした。対数近似の決定係数は 0.77 であり、良い一致が見られた。

Correspondence to: Toshihiro Ozeki,  
ozeki.toshihiro@s.hokkyodai.ac.jp

Copyright ©2024 The Okhotsk Sea & Polar Oceans  
Research Association. All rights reserved.



# Frederick William Beechey's Narrative of the Voyage of the *Blossom* to the Pacific and the Arctic

Gaston R. DEMARÉE<sup>1</sup> and Yoshio TAGAMI<sup>2</sup>

<sup>1</sup>Royal Meteorological Institute of Belgium, Brussels, Belgium

<sup>2</sup>Faculty of Human Development, University of Toyama, Toyama, Japan

(Received October 28, 2023; Revised manuscript accepted January 15, 2024)

## Abstract

Frederick William Beechey's expedition in 1825-1828 was not so much to discover and explore the North Pacific region and Bering Strait but to render assistance to Captain Parry and Captain Franklin. John Franklin was on his second land expedition and was supposed to go westwards from the Mackenzie river to Kotzebue Sound in Alaska. Unfortunately, Beechey had to leave Kotzebue Sound in two consecutive years without having found any trace of Franklin's expedition and sailed back to England having been away for three and a half years but having explored hitherto less known North Pacific and Arctic regions.

**Key words:** Frederick William Beechey, *Blossom*, North Pacific, Bering Strait, Alaska

## 1. Introduction

In 1825 Frederick William Beechey, commander of the sloop *Blossom*, was instructed by the Admiralty to explore uncharted areas of the Pacific, to pass through Bering Strait, and to attempt to make contact there with either an overland expedition from the Mackenzie River, Northwest Territories, led by John Franklin or a naval expedition from Prince Regent Inlet under William Edward Parry. During the summer of 1826 an advance party from the *Blossom* reached as far east as Point Barrow (Alaska) but did not meet either expedition. It was later discovered that the *Blossom*'s party had missed Franklin, who had come within about 150 mi of Point Barrow, by only nine days.

After wintering in the Pacific, F.W. Beechey once more headed north to the Bering Strait in the summer of 1827 but again failed to rendezvous with either Franklin or Parry. He then returned to the Pacific, explored and charted parts of it, and sailed home, reaching Britain in September 1828. The *Narrative of a voyage to the Pacific and Beering's Strait*, was published by authority of the Lords Commissioners of the Admiralty in 1831 (Burant, 1985).

Interesting in this context is also the publication of the *Journal of Lieutenant George Peard of H.M.S. Blossom* (George, 1974; Gough, 2011).

## 2. Frederick William Beechey

### 2.1 His personal life

Frederick William Beechey was born on 17 February 1796 as the son of Sir William Beechey (1753-1839), R.A., R.N., F.R.S. and his second wife, Anne Phyllis Jessop (1764-1833), both of them painters. F.W.

Beechey was a naval officer, an artist, an Arctic explorer, a hydrographer and an author. In December 1828, he married Charlotte, youngest daughter of Lieutenant-Colonel John Stapleton, of Thorp Lee, and they had five daughters. F.W. Beechey was elected President of the Royal Geographical Society, an office which he held from 28 May 1855 until his death. Rear-Admiral Beechey died at his residence, Westbourne crescent, Hyde-Park, on 29 November 1856 (Anonymous, 1857; Murchison, 1857).



Fig. 1 Portrait of Frederick William Beechey painted circa 1822 by his brother George Duncan Beechey.

### 2.2 His naval career

Frederick William Beechey entered the Royal Navy in July 1806, at the age of 10 years, under the direct patronage of Lord St. Vincent, and in 1807 he was rated midshipman. He took part in the attack on New Orleans, and was promoted to lieutenant for a boat operation in

1815. After the Napoleon wars, the British Navy renewed its attempts to discover the northwest passage to the Pacific. In 1818 he was appointed second in command to the brig *Trent* commanded by Lieutenant (afterwards Sir John) Franklin, and had an interesting share in the Arctic expedition of that year. In the next year, 1819, he served again in the Arctic, on board the *Hecla*, under Lieutenant William Edward Parry (Parry, 1828). On 25 Jan. 1822 he had been promoted to the rank of commander, and on 12<sup>th</sup> of January 1825 he was appointed to command the *Blossom*, which was engaged for the next four years in the Pacific, and in endeavoring to co-operate, by Bering's Strait, with the polar expeditions from the eastward. Beechey had been, whilst still in the Pacific in 1827, advanced to the rank of captain. In 1854 Beechey was promoted to rear-admiral. (O'Byrne, 1849; Laughton, 1885; Anonymous, 1857; Burant, 1985)

### 2.3 His Majesty's Ship *Blossom*

H.M.S. *Blossom* was an 18-gun Cormorant-class sloop-of-war which was launched on 10 December 1806 at Robert Guillaume's yard at Northam. She was at Deptford and Woolwich between July 1824 and August 1825 being converted to serve as exploration ship in 'icy seas'. In 1825 Commander Frederick William Beechey commissioned her for exploration of the Pacific Northwest. After the polar expedition, she was at Woolwich being fitted as a survey ship and was recommissioned for the Jamaica station. *Blossom* was hulked as a lazaret at Sheerness in 1833, and was broken up at Chatham in 1848.

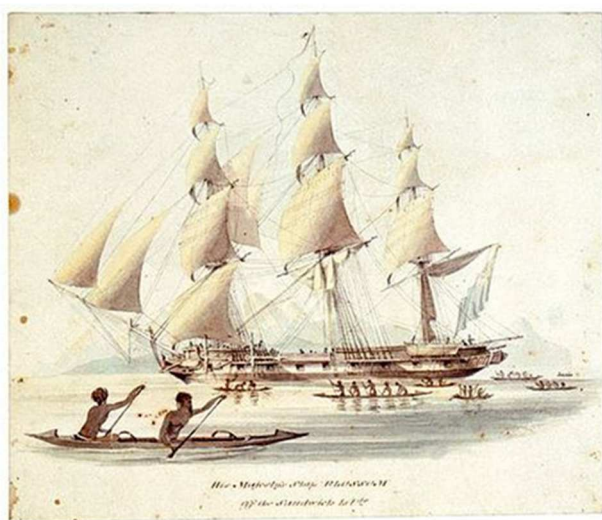


Fig. 2 His Majesty's Ship *Blossom* off the Sandwich Islands.

## 3. Frederick William Beechey's Voyage

### 3.1 The instructions of the Voyage

Frederick William Beechey, Commander of the *Blossom*, received on 11<sup>th</sup> May 1825 at Spithead the

instructions from the Lords Commissioners of the Admiralty that 'under his command H.M.S. *Blossom* should be at Beering's Strait in the autumn of 1826, and, contingently, in that of 1827, for the purpose of affording assistance as may be required, either by Captain Parry or Captain Franklin, should one or both these officers make their appearance in that neighborhood.' Captain Parry should try to discover the north-west passage by way of the Prince Regent's Inlet. At the same time, Captain Franklin should descent the Mackenzie River and coasting the northern shore and arrive at open sea in Bering Strait where F.W. Beechey should await the arrival of both expeditions and, if necessary, provide assistance returning them to Europe. The *Blossom* was strengthened and adapted for that service. 'A boat was supplied, to be used as a tender ... and rigged as a schooner, decked and fitted in the most complete manner.' As the *Blossom* was going to traverse 'a portion of the globe, hitherto little explored' it should survey and explore such parts of the Pacific useful for navigation.



Fig. 3 Track of the *Blossom* in 1825-1828 (frontispiece of Beechey, *Narrative ...*, 1831).

The expedition should stop at Rio de Janeiro to complete provisions and water, sail around Cape Horn to Easter Island, steering for Society Islands [named by Captain James Cook in 1769], proceed to Pitcairn's Island [the island of the Bounty mutiny], on the southeastern extremity of the Society Islands and proceeding north-westerly to Otaheite [Tahiti, the largest island of the Windward Islands of the Society Islands]. Having completed the survey, direct your course to the Navigator's Islands [Samoa Islands], position the Suwarrow's Islands [an island in the northern group of the Cook Islands in the south Pacific Ocean], and 'deliver the dispatches and packages addressed by the Foreign Office for his Majesty's consul at that island, and to procure refreshments and water.' The *Blossom* should not arrive later than 10<sup>th</sup> of July 1826 at the appointed rendezvous and remain there until the end of

October 1826 or as late as the season will admit. In the case that having heard nothing of either of Captains Franklin or Parry, proceed to a place for completing provisions and water and be again in Bering's Strait by the 1<sup>st</sup> of August 1827, staying there as long as possible to not be forced overwintering there on account of the ice, and finally proceed to Spithead, England.

### 3.2 Aspects of the first part of the Voyage

In the beginning of June 1825, the *Blossom* left Oneehow [Niihau, named Oneeheow by Cook, 1778-1779], the westernmost of the Sandwich Islands [Hawaiian Islands], after having taken 'on board as many yams as the natives could collect before sun-set, and then sharpened course to Kamchatka.' 'On the 26<sup>th</sup> June 1825, after having traversed nearly seven hundred miles in thick fog, the horizon was cleared for a few hours' and the temperature fell 31° F lower than it had been thirteen days before. On the next day, they saw the high mountains of Kamchatka and anchored off the town of Petropavlovsk with a magnificent view on the snow-capped volcano emitting smoke in interval. Beechey found dispatches that the sailing expedition of Captain Parry had returned to England and 'desiring to cancel that part of instructions which related to him'.

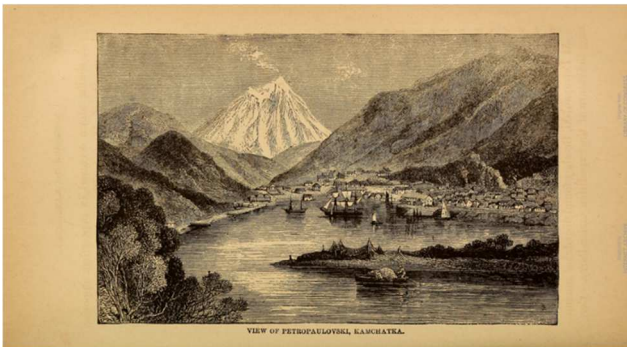


Fig. 4 View of Petropavlovski, Kamchatka (Hyde, Baldwin & Gage, 1874, p. 250).

On the 10<sup>th</sup> of July 1825, Bering Island [the largest of the Commander Islands located about 175 km east of Kamchatka peninsula, 58° 0' N, 166° 16' W], the place where Vitus Bering shipwrecked and found his grave with 28 of his crew in 1741, appeared through the fog. On the 16<sup>th</sup> of July 1825, the *Blossom* stood close into a small bay of St. Lawrence Island [Alaska, U.S.A.] and the crew bartered with the natives [Yupik, Alaskan natives]. The two Diomedes Islands, the Russian Big Diomedede or Ratmarov Island and the U.S. Little Diomedede or Krusenstern Island, were seen and near Schismareff Inlet near the American shore, the natives came off in large skin-covered boats, named *baidars*, and there was good bargaining. 'It was at Schismareff Inlet that they first saw the lip ornaments which are common to all inhabitants of the coast thence as far as Point

Barrow. ... We entered Kotzenue Sound in the morning of the 22<sup>nd</sup> of July ... At four o'clock in the morning of the 25<sup>th</sup> we reached our appointed rendezvous at Chamisso Island ... and there were no traces of Captain Franklin having arrived.'



Fig. 5 Track of the first part of the voyage of the *Blossom* to Bering Strait in 1825.

On the 30<sup>th</sup> of July 1825, the *Blossom* attended by the barge, in command of Elson, weighed from Chamisso Island and steered out of the Kotzebue Sound to proceed surveying the coast to the north looking for traces of Franklin's land expedition. There were visits to the *Blossom* and to the barge by the natives, who were friendly. At specific places, a bottle was deposited with indications to find it. On the 13<sup>th</sup> August, 1825, they were at latitude 71° 07' N, longitude 163° 40' W, on the land a post was put up for the land expedition, and a bottle buried near. The boat had proceeded to the latitude 71° 23' 31" N and to 156° 21' 30" W and had to return because the whole body of ice was moving to the land. This farthest tongue of land which they reached was named Point Barrow by Beechey and is only 146 miles from the extreme of Franklin's progress westward from the Mackenzie River. Finally, the *Blossom* left Kotzebue Sound and sailed to San Francisco for overwintering arriving on November 7<sup>th</sup>, 1825, in San Francisco harbor.



Fig. 6 Baidars of Hotham Inlet with native Alaskans (Beechey, *Narrative ...*, 1831, p. 250).

### 3.3 Aspects of the second part of the Voyage

On the 5<sup>th</sup> of January, 1827, the *Blossom* put to sea to the Sandwich Islands which were arrived after a passage of 20 days. On the 4<sup>th</sup> of March, they left for Macao, China, to get medicines. They passed on the 15<sup>th</sup> March Wake's Island, on the 25<sup>th</sup> March Assumption, on the 7<sup>th</sup> of April Bashee Islands [a group of Philippine islands between Luzon and Formosa] and arrived on the 10<sup>th</sup> of April at the Tupa/Taipa anchorage in Macao. It was decided to change the water in Napakang [Napa River] on Great Loo Choo [Great Lew-Chew, Ryūkyū Islands]. At Naha, the *Blossom* was inspected by an officer, then followed by several well-dressed persons who made inquiries on the ship and the reason of the visit. One of the party, the so-named linguist An-Ya 'recollected the visit of the *Alceste* and the *Lyra*, which he correctly said was 144 moons ago [15 Sep. – 9 Nov. 1816]. ... An-Ya said that Loo Choo had been visited by a violent typhoon in April, which unroofed the houses and did much other mischief.' 'On the 25<sup>th</sup> of May 1826 we took our departure from Loo Choo'. They took possession of an uninhabited island named it Peel Island of the Arzobispo group [Bonin-sima, Japan], and its harbor Port Lloyd [27° 05' 35" N, 217° 45' 54" W].



Fig. 7 Track of the second part of the voyage of the *Blossom* to Bering Strait in 1827 and return to England in 1827-1828.

'On the 2<sup>nd</sup> of June we made the snowy mountains of Kamchatka. ... The season was more backward than in the preceding year; and though it was beginning of July, the snow lay deep upon some parts of the shore.' 'On the 1<sup>st</sup> of August, we apprised our approach of St. Lawrence Island. ... About midnight the temperature of the water fell to 31°, and soon after that of the air was reduced from 42° to 34°.' On the 5<sup>th</sup> of August, the *Blossom* came to an anchor off Camisso Island. 'The line of packed ice, in the meridian of Icy Cape [70° 19' 47" N, 161° 52' 27" W], was twenty-four miles to the southward of its position the preceding year.' The barge under command of Lieutenant Belcher was shipwrecked and three members of the crew drowned. In the beginning of

October, sharp frosts and heavy snowfall came, and no intelligence of Captain Franklin's expedition had been received, Beechey decided to quit the anchorage in Kotzebue Sound and to sail south, mooring in the Bay of Monterey on the 29<sup>th</sup> of October 1827.

### 4. Nautical, geographical, magnetical and meteorological Observations

The Annex of the 1831-version of the *Narrative of a voyage to the Pacific and Beering's Strait* contains nautical, geographical, magnetical and meteorological observations. In the places where the *Blossom* remained a long time, precise geographical positions have been determined and compared to known results (Table I). At the same places, the elevation of specific items was ascertained by barometric or by trigonometric techniques (Table II). The meteorological tables contain a table of the daily 3-hourly barometer observations but the daily mean mercury temperature values are only means for every five degrees of latitude on each side of the equator and in the extra-tropical latitudes to every five or six days (Table IV). Table VI presents the meteorological observations of temperature of air and surface of the sea, humidity of the atmosphere, wind, weather and clouds. However, the geographical coordinates are only given at 5° latitudes and 1° longitudes. Table IX provides the specific gravity of sea water (in grains) and temperature. Tables XI and XII contain magnetical observations.

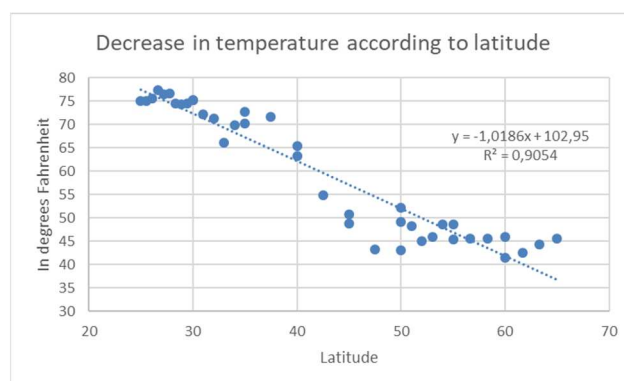


Fig. 8 Decrease of the temperature according to the latitude.

Figure 8 show the decrease of the daily temperature between the latitude 25 to 65 providing a, approximate decrease of 1° F per 1° latitudes. However, the decrease is different in the lower and in the higher altitudes. In the lower latitudes it remains approximately 1° F per unit latitude where it lowers to approximately 0.6° F per latitude in the higher latitudes.

### 5. Conclusion

In the years 1825-1828, the English sloop *Blossom* made a three years long voyage through the Pacific and

Bering Strait. The instructions from the Lords Commissioners of the Admiralty provided assistance to Captain Parry on his voyage searching the North-West passage from Prince Regent's Inlet and/or Captain John Franklin land expeditions descending the Mackenzie River might one of these expeditions reach the area where Beechey was waiting for them. In the summer of 1825, Captain Franklin went downriver and reached its mouth. In the following summer, Franklin found the ocean frozen and worked his way west for several hundred miles and gave up on 16 of August 1826 at Return Reef, a single island NE of Gwydyr Bay, at about 150 mi (240 km) east of Point Barrow, and began to retrace his way towards the Mackenzie River.

The Narrative of the Voyage isn't a logbook and misses much of the nautical, scientific, meteorological and geographical information usually contained in the Captain's record. In this case, the geographical coordinates are generally given in the approximations of 1 to 5 degrees' latitude and 1-degree longitude which do not allow geographical, meteorological and geophysical research.

On the other hand, the Narrative contains interesting information on the native Alaskans which was welcomed in the early 19<sup>th</sup> century by the reading public and provided several successful reprints and translations of the Narrative.

### Acknowledgements

The authors sincerely acknowledge the constructive remarks and suggestions made by two anonymous reviewers. The authors are also grateful to prof. emer. Dr. Shuhei Takahashi for his precious help in the production of this paper.

### References

- Anonymous (1857): Obituary, Admiral Beechey, F.R.S. The Gentleman's Magazine and Historical Review. M DCCC LVII, January to June inclusive, London, John Henry and James Parker, 108-110.
- Anonymous (1910): Beechey, Frederick William. The Encyclopaedia Britannica, A Dictionary of Arts, Sciences, Literature and general Information, Eleventh Edition, Volume III, Cambridge, England, University Press, p. 640.
- Beechey, F.W. (1831): *Narrative of a Voyage to the Pacific and Beering's Strait, to co-operate with the Polar Expeditions. Performed in his Majesty's Ship Blossom, under the Command of Captain F.W. Beechey, F.R.S., F.R.A.S., and F.R.G.S. in the Years 1825, 26, 27, 28.* In two Parts, London, Henry Colburn and Richard Bentley, 742 p.
- [Beechey, F.W. (1831)]: Review of Narrative of a Voyage to the Pacific and Beering's Strait, to co-operate with the Polar Expeditions. Performed In his Majesty's Ship Blossom, under the command of Captain F. W. Beechey, R. N. in the Years 1825, 26, 27, 28. *The Quarterly Review*, April 1831, **45**, 57-97.
- Burant, J. (1985): *Beechey, Frederick William*, Dictionary of Canadian Biography, Vol. VIII, 1851-1860. Toronto, 70-71.
- Gough, B.M. (2011): *To the Pacific and Arctic with Beechey: The journal of lieutenant George Peard of HMS Blossom, 1825-1828. To the Pacific and Arctic with Beechey: The Journal of*

- Lieutenant George Peard of HMS Blossom, 1825-1828*, 272 p.
- Hyde, A., Baldwin, A.C., and Gage, W.L. (1874): *The frozen zone and its explorers; a comprehensive record of voyages, travels, discoveries, adventures and whale-fishing in the Arctic regions for one thousand years. With a ...* Hartford, Conn., Columbian Book Company, 800 p.
- Laughton, John Knox (1885): *Beechey, Frederick William*. In: Stephen, Leslie (ed.) *Dictionary of National Biography*, Vol. 4. London, Smith, Elder & Co, 121-122.
- Murchison, R.I. (1857): Address to the Royal Geographical Society of London; delivered at the anniversary meeting on 25th May, 1857, By Sir Roderick Impey Murchison, G.C.ST.S., D.C.L., F.R.S., &C. *Journal of the Royal Geographical Society*, **27**, xciv-cxix.
- O'Byrne, William R. (1849): *Beechey, F.R.S., &c.* In: A naval biographical dictionary: comprising the life and services of every living officer in Her Majesty's navy, from the rank of admiral of the fleet to that of lieutenant, inclusive. London, John Murray, 66-67.
- Parry, W.E. (1828): Narrative of an Attempt to reach the North Pole in boats fitted for the Purpose, and attached to His Majesty's Ship Hecla, in the Year MDCCCXXVII, under the Command of Captain William Edward Parry, R.N., F.R.S., ... London, John Murray, 229 p.

### Summary in Japanese

和文要約

### F. W. ビーチェイによる 太平洋と北極へのブロッサム号の航海

Gaston R. DEMARÉE<sup>1</sup>, 田上善夫<sup>2</sup>

<sup>1</sup>ベルギー王立気象研究所, <sup>2</sup>富山大学

北極北西航路が未発見であった頃、1825年から1828年にかけてのF. W. ビーチェイの太平洋側から北極海へ向かう航海は、グリーンランド側から船で北西航路発見に向かうパリー隊とカナダ内陸から北極海へ向かうフランクリン隊を支援することが目的だった。また北太平洋地域とベーリング海峡を越えた北極地域を探検する目的もあった。フランクリンは二度目のカナダ内陸地域探検であり、マッケンジー川を下ってアラスカのコツェビュー湾まで西に向かうことになっていた。残念ながら、ビーチェイはフランクリン隊と会えないまま、2年連続でコツェビュー湾を離れなければならなかった。しかし、それまであまり知られていなかったアラスカ北極地域と北太平洋地域を調査することができた。

(編集部注)：その後、1845年にフランクリン隊総勢129名は2隻の船で北西航路に向かったが全員死亡した。フランクリン隊が最初に越冬したビーチェイ島は、このF. W. ビーチェイ船長の名に由来する。

Correspondence to: G. R. Demarée,  
gaston.demaree@meteo.be

Copyright ©2024 The Okhotsk Sea & Polar Oceans Research Association. All rights reserved.



## Submission Information for OSPOR

### Reviewing processes of OSPOR

- 1) When manuscripts have been received by the Editor-in-Chief, an acknowledgement of receipt will be sent to the author(s) by e-mail. The Editor-in-Chief chooses an editor to handle the manuscript review.
- 2) The submitted manuscript will be subjected to screening review for its scope, novelty, completeness, English level, and conformation to the OSPOR policy. A manuscript not passing the screening review will immediately be returned to the authors.
- 3) The editor in charge will select expert reviewers to evaluate the manuscript.
- 4) As to results of review, if the editor decides that the paper needs revision by the author(s), the manuscript will be returned to the author(s) for revision.
- 5) Manuscripts returned to author(s) for revision should be resubmitted promptly. If the revision cannot be finished within a month, the manuscript will be regarded as having been withdrawn.
- 6) The Editor-in-Chief will finally decide whether to accept the manuscript for publication.

### Paper Submission

#### Submission Guideline

All manuscripts should be submitted in digital format (PDF or WORD) with the OSPOR submission sheets (PDF or WORD, offered from OSPOR) by email to the OSPOR Editorial Board

#### OSPOR Editorial Board

Polar Oceans Research Association (OSPORA)  
Address: Kaiyo Koryukan, Kaiyo Koen 1, Mombetsu, Hokkaido 094-0031  
Japan E-mail: momsys(at)okhotsk-mombetsu.jp  
Phone: +81-158-26-2810 (0158-26-2810 in Japan)  
Fax: +81-158-26-2812 (0158-26-2812 in Japan)

#### Publication Charge

Authors of their institutions are requested to pay the publication charge according to the following rate when paper is accepted. The maximum pages are 6 pages.

- 1,500 Yen / page within the maximum pages
- 3,000 Yen / page over the maximum pages (Excess charge)

#### Copyright

Copyright for an article submitted to OSPOR is transferred to OSPORA when the article is published in OSPOR in any form.

#### Preparation of manuscripts

The manuscript should be formatted in the form of OSPOR template offered from the OSPORA office, which satisfies the following requirements. The maximum pages in printing style are **6 pages**. Otherwise, an overage fee will be charged.

- 1) Text
  - a) The manuscript should be in the international size A4 in camera-ready style according to the form of OSPOR template.
  - b) The first page should include: the title, the author(s) name(s) and their affiliations. If possible, a Japanese translation of the title and the name(s) of the author(s) should be provided in the end of manuscript. If they are not, the translation will be undertaken by the OSPOR editorial board.
  - c) An abstract not exceeding 250 words must be provided.
  - d) Up to five keywords that describe the content for indexing purposes must be provided.

## 2) References

a) A list of cited references should be arranged alphabetically. Journal abbreviations are better to use, but when the abbreviation is not known, the full title of the journal should be used in the list.

In the case of many authors, the author's name can be written in short as below.

Kawamura, K., F. Parrenin and 16 co-authors (2007): Northern hemisphere forcing of climatic cycles in Antarctica over the past 360,000 years. *Nature*, **448**, 912-916.

b) References in the text will include the name(s) of the author(s), followed by the year of publication in parentheses, *e.g.* (Clark, 2003), (Li and Sturm, 2002), (Harrison *et al.*, 2001).

## 3) Units

Numerical units should conform to the International System (SI).

Units should be in the form as kg m<sup>-3</sup> not as kg/m<sup>3</sup>.

## 4) Tables

A title and a short explanation should be located on the top of table.

They should be referred to in the text.

## 5) Figures

a) All Figures (illustrations and photographs) should be numbered consecutively.

b) All Figures should be of good quality and referred to in the text.

c) Figure captions should be located on the bottom of the Figures.

## 6) More information

For more information about manuscript instruction, please ask to OSPORA office or see OSPORA home page in <http://okhotsk-mombetsu.jp/okhsympo/top-index.html>

## Recent information

Recent information can be get from Symposium HP:

<http://www.okhotsk-mombetsu.jp/okhsympo/top-index.html>

## **Organized and sponsored by**

City of Mombetsu  
Arctic Research Center, Hokkaido University (ARC)

Okhotsk Sea and Polar Oceans Research, Vol. 8 (2024, February)

Published by the Okhotsk Sea and Polar Oceans Research Association (OSPORA),  
Mombetsu City, Hokkaido, Japan

### **Executive Committee of OSPORA:**

Chairman: Shuhei Takahashi (Okhotsk Sea Ice Museum of Hokkaido, Director)

Secretariat: Eriko Uematsu

Address: Kaiyo Koryukan, Kaiyo Koen 1, Mombetsu, Hokkaido 094-0031

Japan E-mail: momsyst(at)okhotsk-mombetsu.jp

Phone : +81-158-26-2810 (Japan 0158-26-2810)

Fax: +81-158-26-2812 (Japan 0158-26-2812)

<http://okhotsk-mombetsu.jp/okhsympo/top-index.html>



## Okhotsk Sea and Polar Oceans Research

Published by the Okhotsk Sea and Polar Oceans Research Association (OSPORA)  
Mombetsu City, Hokkaido, Japan